CALIFORNIA STATE UNIVERSITY, NORTHRIDGE

Experimental Study of Bubble Dynamics During Pool Boiling of Nanofluids

A thesis submitted in partial fulfillment of the requirements

for the degree of Master of Science

in Mechanical Engineering

By

Burla Goutham Kumar Reddy

August 2018

The thesis of Burla Goutham Kumar Reddy is approved by

	Date
Dr. Shadi Mahjoob	
	Date
Dr. Vibhav Durgesh	
	Date
Dr. Abhijit Mukherjee, Chair	

California State University, Northridge

Dedication

This work is dedicated to my father Dr. Burla Siva Kumar Reddy and my mother Burla Aparna, for their love and inspiration.

I am thankful to my advisor, Dr. Abhijit Mukherjee for giving me this opportunity. His unconditional support and motivation helped me in exploring and learning new things.

I would also like to thank, Dr. Shadi Mahjoob and Dr. Vibhav Durgesh for being part of my thesis committee and for their valuable feedback on my thesis.

Table of Contents

List of Tables

List of Figures

Nomenclature

B	horizontal length of the bubble
C	vertical length of the bubble
C_p	Specific heat
D	diameter of the bubble
g	gravitational constant
h_{fg}	latent heat of evaporation
k	thermal conductivity
M	molecular weight
ms	milliseconds
p	pressure
P_c	critical pressure
R_p	roughness parameter
Pr	prandtl number
q''	heat flux
T	temperature
ΔT	superheat, $T_w - T_{sat}$

t	time
t_g	growth time of the bubble
U	uncertainty
V	volume
x_1	distance between thermocouples
x_2	distance between copper surface and second thermocouple

Greek symbols

μ	dynamic viscosity
ρ	density
σ	surface tension
ϕ	concentration by volume
ω	concentration by weight
γ	constant
λ	thermal conductivity
θ	bubble contact angle

Subscripts

b	bubble base

Cu	copper
Eq	bubble equivalent
f, l	liquid
g, v	vapor
p	nanoparticle

Abstract

Experimental Study of Bubble Dynamics During Pool Boiling of Nanofluids

By

Burla Goutham Kumar Reddy

Master of Science in Mechanical Engineering

Nanofluids are stable colloidal suspensions of nanometer sized particles suspended in traditional heat transfer fluids. During boiling of nanofluids, the dispersed nanoparticles change the surface conditions on the heated surface. A layer of nanoparticles is expected to be deposited on the surface during the boiling process which affects the boiling characteristics and the critical heat flux. The deposition of nanoparticles on the surface changes the surface contact angle as well as the bubble growth rates. In this study, nucleate pool boiling experiments have been performed using 10 nm and 30 nm sized alumina nanoparticles dispersed in water at 10^{-4} vol% and 10^{-3} vol% concentrations. A deterioration in heat transfer was observed during boiling of nanofluids. As bubbles nucleate from the copper surface, the entire bubble growth cycle has been visualized and recorded using a high-speed camera. For each concentration of nanofluid, bubble growth period, bubble equivalent, and base diameters, and the bubble contact angle have been measured. This measured data was compared with measurements obtained during pool boiling of base fluid water.

CHAPTER I. INTRODUCTION

Background and Motivation

High-performance cooling is one of the most significant needs in many industrial applications. Boiling is one of the efficient modes of heat transfer and is encountered in many thermal management systems. The demand for even higher cooling heat fluxes is increasing with the advancement and miniaturization of current systems. In various efforts to enhance heat transfer, significant improvements have been constrained because of the traditional heat transfer fluids like water, oils and ethylene glycol, which have poor thermal conductivities. To improve the thermal conductivity of these liquids, previous research and development efforts were made by adding millimeter- or micrometer-sized solid metallic particles in fluids. This century-old technique has a significant limitation of rapid settling, and moreover, such millimeter- or micrometer-sized particles are not applicable to the emerging microsystems.

The advancement in nanotechnology, enabled the production of nanometer-sized metallic and non-metallic particles and a new class of engineered working fluids called 'nanofluids' have emerged. Nanofluids are stable colloidal suspensions of nanometer-sized particles (less than 100 nm) suspended in traditional heat transfer fluids. Commonly used nanoparticles are alumina, copper oxide, silica, copper, iron, silver, gold, CNT, and diamond.

Over the past decade, nanofluid technology has mainly developed with many experimental and numerical studies on heat transfer using nanofluids. Various research

groups have investigated the effect of nanoparticle addition during pool boiling. Majority of these studies reported that the nanofluids are enhancing the critical heat flux, but there is no explicit agreement on the effect of nanoparticle addition on pool boiling heat transfer coefficient. Few studies reported that the nanoparticles deposit on the surface and activate multiple nucleation sites, thereby improving boiling performance. Others have stated that the same nanoparticle deposition leads to deterioration of heat transfer. To better understand the potential use of nanofluids in pool boiling applications, it is necessary to know the bubble formation, growth, and the underlying heat transfer mechanisms.

Pool Boiling

Pool boiling is a boiling process occurring on a heated surface submerged in a large volume of stagnant liquid. The pool boiling is best described experimentally by the boiling curve as shown in Fig 1.

In the natural convection boiling regime, the liquid near the heated surface rises to the free surface of the pool by natural convection currents. This natural convection continues till the fluid near the surface gets superheated to a point A as shown in Fig 1. The point A is referred as the onset of nucleate boiling (ONB), where isolated bubbles begin to form. If the vapor bubbles form in the superheated bulk fluid, it is called homogeneous nucleation. This type of nucleation requires a higher degree of superheat temperatures and is not quite standard during boiling. The commonly encountered heterogeneous nucleation process refers to the formation of bubbles in the presence of pre-existing vapor nuclei at the pits, grooves or scratches on the heated surface. Hence, the

heater physical and chemical conditions influence the heterogeneous nucleation and growth of bubbles.

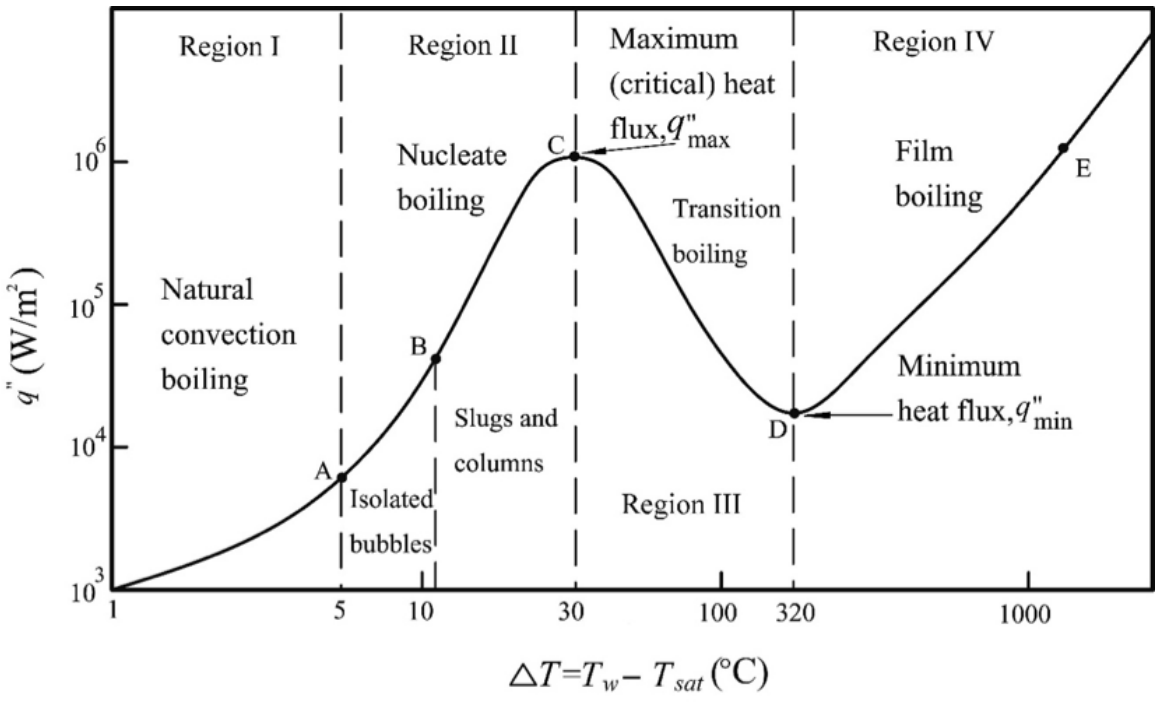

Figure 1 Typical pool boiling curve [1]

As the heat flux increases, more and more nucleation sites get activated and a transition from isolated bubbles to vapor patches and columns can be observed. From point B-C, a well-established nucleate boiling can be witnessed, and as heat flux increases, the formation of vapor columns is intensified until it reaches point C (critical heat flux). This point sets the upper limit to nucleate boiling regime and is also referred to as departure from nucleate boiling (DNB). The segment C-D is unstable and may oscillate between nucleate boiling and film boiling. The formation of an unsteady blanket of vapor has an insulating effect on the surface which decreases the heat flux and heat transfer. Point D is called the Leidenfrost point and represents the onset of film boiling. At this point, the heat flux is minimum, and formation of a stable vapor blanket can be noticed. During film

boiling (D-E), the vapor blanket completely covers the surface and radiation from the heated surface through the vapor begins to dominate. Point E is called the burnout point, at which the surface begins to melt.

Nucleate boiling correlations

Nucleate boiling is a complex regime and modelling this regime is heavily based on various empirical correlations and mechanistic models. Rohsenow [2] proposed a correlation to predict the heat flux as function of wall superheat by formulating the phase change process as single-phase forced convection. Rhosenow suggested that the heat removal is due to the liquid motion caused by the departing vapor bubbles. He used the bubble departure diameter and the vapor superficial velocity, to relate the Nusselt number to Reynolds number. The widely used form of the Rohsenow correlation is:

$$q'' = \mu_f h_{fg} \left[\frac{g(\rho_f - \rho_g)}{\sigma}\right]^{\frac{1}{2}} \left[\frac{C_{pf}\Delta T}{C_{sf} h_{fg} {Pr_f}^n}\right]^3 \quad (1)$$

Where the constant C_{sf} is depended on the heat material and fluid combination. The exponent n is given a value of 1 for water and 1.7 for other liquids.

A comprehensive correlation for saturated nucleate pool boiling of different liquids was proposed by Stephan and Abdelsalam [3]. The Nusselt numbers were related to several dimensionless parameters that depend on properties of fluids and solids. They have grouped the liquids into: water, hydrocarbons, cryogenic liquids, and refrigerants. These correlations were developed by using the data obtained from various heater geometries. In addition, a mean surface roughness of 1 micron was assumed for all the heaters.

The generalized correlation, which is applicable to all the liquids is:

$$\frac{\mathrm{q}D_d}{\Delta T\lambda_l} = 0.23\left(\frac{\mathrm{q}D_d}{\lambda_l T_{Sat}}\right)^{0.674}\left(\frac{\rho_v}{\rho_l}\right)^{0.297}\left(\frac{h_{fg}D_d^2}{k_l^2}\right)^{0.371} \times\left(\frac{\rho_l-\rho_v}{\rho_l}\right)^{-1.73}\left(\frac{\alpha_l^2\rho_l}{\sigma D_d}\right)^{0.371} \quad (2)$$

Where D_d is the bubble departure diameter

The surface roughness, molecular weight and reduced pressure are considered as the correlating parameters by Cooper [4]. The correlation is much simpler and easy to use. But this model does not account for the variation in degree of surface wettability. The cooper correlation for a flat plate can be written as:

$$\frac{q^{\frac{1}{3}}}{\Delta T} = 55.0\left(\frac{p}{p_c}\right)^{0.12-0.21\log_{10}R_p}\left(-\log_{10}\frac{p}{p_c}\right)^{-0.55}M^{-0.50} \quad (3)$$

Where R_p is the surface roughness in microns.

CHAPTER II. LITERATURE REVIEW

Pool Boiling of Nanofluids: Experimental Studies on HTC

Since 2003, various research groups have been investigating the pool boiling characteristics of nanofluids. Das et al [5] conducted pool boiling experiments using Al_2O_3 nanoparticles dispersed in water at 1%, 2% and 4% volume concentrations. The boiling surfaces were 20mm diameter horizontal cartridge heaters with different surface roughness and they have observed pool boiling curves of nanofluids shifting towards the right. The authors concluded that the reason behind the degradation of heat transfer was caused by nanoparticle deposition, which made both the heater surfaces smoother. In an another study by the same authors, Das et al [6] studied the effect of nanoparticles during pool boiling, by using narrow tubes with diameters of 4mm and 6.5mm. They have observed deterioration of heat transfer due to the decrease of nucleation site density caused by the deposition of nanoparticles.

Tirsaksri & Wongwises [7] used TiO_2 nanoparticles dispersed in R141b, and conducted pool boiling experiments at various pressures ranging from 200 KPa to 500 KPa. A horizontal copper cylinder was used as the heating surface and the TiO_2/R141b nanofluids concentration varied from 0.001 vol% to 0.05 vol%. Independent of pressure, the heat transfer coefficients of nanofluids were found to be lower than the base fluid. Sarafraz & Homozi [8] conducted pool boiling experiments using stainless steel cylinder as the heating surface. They have studied the pool boiling heat transfer characteristics of Al_2O_3/ Ethylene glycol nanofluid at dilute concentrations ranging from 0.1-0.3 wt%. In

their study, they observed a decrease in heat transfer coefficients (HTC) of nanofluids when compared to the base fluid. Pool boiling heat transfer characteristics of refrigerant based nanofluids was studied by Naphon & Thongjing [9]. They dispersed TiO_2 nanoparticles in ethyl alcohol and R141b at a concentration range of 0.01-0.075 vol%. They observed deterioration in heat transfer coefficient with increase of nanofluid concentration.

Unlike the above specified studies, some experimental investigations reported enhancements in pool boiling heat transfer coefficients using nanofluids. Wen & Ding [10] investigated pool boiling of aqueous based alumina nanofluids at various concentrations. The authors did not observe any deposition of nanoparticles on the steel heating surface after boiling with nanofluids. They reported a 40% increase in heat transfer coefficient of nanofluid (1.25 wt %), when compared to pure water. Soltani et al [11] conducted pool boiling experiments by dispersing Al_2O_3 and SnO_2 nanoparticles in water at 0.3-2 wt% and 0.5-3 wt% respectively. They observed enhancement in heat transfer varying with the type and concentration of nanofluid. The authors reported a 30% increase in HTC of Al_2O_3/water nanofluid (2 wt %) and 20% increase for SnO_2/water nanofluid (3 wt%), when compared to pure water. Heris [12] observed HTC enhancement with increasing nanofluid concentration. The author used CuO/Ethylene glycol-water nanofluid at a concentration range of 0.1 to 0.5 wt%. At a nanofluid concentration of 0.5 wt%, 55% enhancement in heat transfer coefficient was reported. Kole & Dey [13] studied thermophysical and pool boiling characteristics of ZnO nanoparticles dispersed in ethylene glycol. They tested ZnO/ethylene glycol at 0.35-2.6 vol% concentrations. The authors observed an increase in heat transfer coefficient of up to 22% with the 1.6 vol% nanofluid. Sodium Dodecyl Benzene Sulfonate (SDBS) dispersant was used by Raveshi et al [14], to stabilize the

alumina/water-ethylene glycol nanofluid. They used copper plate as the heating surface and when compared to the binary mixture of Water-Ethylene Glycol, the HTC improved with nanofluids for all concentrations. The nanofluids tested were in the concentration range of 0.005-1 vol% and an increase of 64% in HTC of the 0.75% nanoparticle volume concentration was reported.

Due to the addition of nano particles, both enhancement and deterioration in heat transfer was observed by some research groups. Narayan et al [15] defined a surface-interaction parameter which is the ratio of the average surface roughness to the nanoparticle diameter by conducting pool boiling experiments with alumina-water nanofluids on vertical stainless steel tubes. If the surface-interaction parameter is less than 1, particle size is more than roughness value and vice versa. They observed both enhancement and deterioration of heat transfer depending on the surface roughness, nanofluid concentration and particle size. The authors have reported a 70 % enhancement of heat transfer when compared to water, when the parameter is 10.48(R_a = 524 nm, d_P = 47nm) and observed deterioration in boiling performance when the parameter is near unity (R_a = 48nm, d_P = 47nm). They mentioned that the deposition of the nanoparticles which are nearly the size of the existing nucleation sites, significantly reduce the number of the active nucleation sites and deteriorate the heat transfer. When the nanoparticles size is much smaller than size of the nucleation sites, the deposition of nanoparticles creates multiple nucleation sites and hence could enhance heat transfer. Pool boiling experiments were performed using ZrO2-water nanofluids by Chopkar et al [16]. The experiments were conducted on a 60.5mm diameter copper plate with nanofluid concentrations from 0.005 vol% to 0.15 vol%. The authors observed substantially higher boiling heat transfer

coefficient at lowest concentration of nanofluid (0.005 vol%), but the boiling heat transfer degraded with increase in concentration. They mentioned that the decrease in heat transfer coefficient is due to smoothening of surface with addition of nanoparticles. Suriyawong & Wongwises [17] conducted nucleate pool boiling experiments using TiO_2/water nanofluids at very low concentrations ranging from 0.00005 vol% to 0.01 vol%. Copper & aluminum surfaces with different surface roughness (0.2 µm and 4 µm) were used as heaters. Independent of nanofluid concentration, the HTC of nanofluids on the aluminum surfaces, were found to be less than that of water. The heat transfer coefficient of 0.0001 vol% nanofluid, when compared to that of water increased by 15% and 4% for copper surfaces with surface roughness of 0.2 µm and 4 µm respectively.

Wen et al [18] investigated the effects of nanofluids on boiling heat transfer and heating surface. Brass plates with different surface roughness (25 nm & 420 nm) were used as heaters. Pool boiling experiments were conducted using Al_2O_3/water nanofluids at low concentrations of 0.001 vol%, 0.01 vol% and 0.1 vol%. The experimental results revealed a two-fold increase in HTC of 0.001 vol% nanofluid for smooth surface at low heat fluxes. For rough surface, the HTC of nanofluid remained the same as that of water. Atomic force microscope (AFM) and Scanning electron microscope (SEM) images of the surfaces after boiling showed nano particle coating. In an another study, Wen [19] observed similar enhancement and deterioration of heat transfer by Al_2O_3/water nanofluids on copper blocks with different surface roughness. When compared to water, a two-fold increase in HTC was observed for smooth surface (R_a=25 nm) and no change for rough surface (R_a=420 nm) with 0.001% nanofluid.

Ahmed & Hamed [20] conducted pool boiling experiments using Al_2O_3/water nanofluids on a copper surface with average surface roughness of 50 nm. They observed no change in heat transfer when alumina nanoparticles are added in water at 0.1% volume concentration. The 0.01 vol% nanofluid enhanced the rate of heat transfer when compared to water. The higher concentrated nanofluid (0.5 vol%) deteriorated the heat transfer. The authors observed nanoparticle deposition on the copper surface after pool boiling with nanofluids. Xu & Zhao [21] studied the effect of nanofluids on heat transfer in porous materials. Copper foam structures with different pore densities and porosities were investigated under pool boiling conditions. Al_2O_3/water and SiC/water nanofluids were used at different concentrations from 0.01 vol% to 1 vol%. Enhancement or deterioration in heat transfer was observed depending on the foam structure and concentration of nanofluid. Tang et al [22] investigated the nucleate pool boiling heat transfer characteristics of Al_2O_3/R141b nanofluid with and without Sodium Dodecyl Benzene Sulfonate (SDBS) surfactant. The nanofluid with the addition of surfactant increased the heat transfer coefficient up to 48%, when compared to pure water. The 0.1 vol% nanofluid without surfactant decreased the HTC by 19%. Similar results were obtained by Sarafraz & Hormozi [23] for CuO/water nanofluid with the addition of surfactant. They conducted experiments by adding three kinds of surfactants namely SDS, SDBS & TritonX-100 by 0.1 wt% to the nanofluids. When compared to water, addition of surfactant to the nanofluid enhanced the HTC. Whereas, deterioration in HTC was observed with nanofluids without surfactants.

Cieslinski & Kaczmarczyk [24] dispersed Cu and Al_2O_3 nanoparticles in water, to conduct pool boiling experiments at various pressure conditions (10 KPa to 200 KPa) on

smooth and porous coated stainless steel tubes. Independent of pressure, both the nanofluids have enhanced heat transfer for smooth tubes. In the case of 0.15 mm thick aluminum porous coating with mean pore radius of 2.8 μm, the addition of nanofluids deteriorated the heat transfer. They mentioned that this deterioration could be due to the deposition of nanoparticles inside the porous matrix and hence reducing the active nucleation sites. Sayahi & Bahrami [25] conducted experiments using ZnO/water, Al_2O_3/water & SiO_2/water nanofluids at 0.03 wt% concentration. They studied the combined effect of nanofluid and surfactant on heat transfer by addition of SDS at 0.01 wt%. An enhancement in heat transfer of about 56.98% was observed with ZnO+SDS/water nanofluid. While SiO_2/water nanofluid deteriorated the heat transfer by 20.63%. Al_2O_3/water nanofluid without SDS enhanced heat transfer by 56.20% and with SDS addition, 48.17% enhancement in heat transfer was reported.

Pool Boiling of Nanofluids: Experimental Studies on CHF

Most of the literature on pool boiling of nanofluids reported that the CHF was enhanced when the nanoparticles are dispersed in a base fluid. You et al [26] were the first to report a 200% increase in critical heat flux (CHF) when Alumina nanoparticles were mixed in water. They conducted experiments at a pressure of 2.89Psia, using a 1x1 cm^2 polished copper surface. The nanofluid concentrations ranged from 0.001g/L to 0.05g/L. They observed an increase in CHF in all the cases but no change in the boiling heat transfer coefficients. The authors could not explain the increase in CHF with any existing model but stated that the bubble sizes are approximately 30% larger due to nanoparticles and they departed with lesser frequency. In a study by Vassallo et al [27], silica nanoparticles which are 50nm in diameter were diluted in water at 0.5% by volume concentration. The maximum heat flux was three times more than that of water. They observed a silica coating of 0.15 – 0.20 mm thick on the NiCr wire after boiling with nanofluid and the wire has sustained film boiling regime at temperatures close to the melting point of the wire. Bang & Chang [28] conducted pool boiling experiments on a 4 x 100 mm^2 copper plate using Al_2O_3/water nanofluids. The concentrations of nanofluids ranged from 0.5 to 4 vol%. The addition of nanoparticles degraded the boiling heat transfer when compared to pure water. They studied the effect of nanofluids on critical heat flux at both horizontal and vertical surface orientations. In the horizontal case, an increase of 32% in CHF was observed and when the surface was in vertical direction, a 13% increase in CHF was reported. They observed a change in roughness due to the deposition of nanoparticles and they mentioned that this surface coating effect reduced the active nucleation sites and provided large vapor blankets, delaying CHF. Kim et al [29] conducted pool boiling experiments using NiCr, Ti

wires of 0.2mm and 0.25 mm in diameters respectively. Water based nanofluids with titania and alumina nanoparticles at concentrations of 10^{-5} to 10^{-1} in volume were investigated. They reported an increase in CHF using nanofluids when compared to water. For concentrations below 10^{-3} vol%, TiO_2/water nanofluids increased CHF by 148% and the Al_2O_3/water nanofluids enhanced CHF by 176%. These enhancements were observed on both the wire materials and the authors reported that the nanoparticle deposition is the primary reason for this increase in CHF.

Water based nanofluids with Al_2O_3, ZrO_2 and SiO_2 nanoparticles at concentrations from 0.001 vol% to 0.1 vol% was investigated by Kim et al [30]. The experiments were conducted on a stainless-steel wire of 0.38 mm diameter. The nanofluids decreased the boiling heat transfer coefficients, but enhanced the critical heat flux. The authors observed an increase of 52%, 75% and 80% with Alumina, Zirconia and Silica nanoparticles respectively. The Scanning Electron Microscope (SEM) images confirmed a porous layer on the wire after nanofluid boiling. A stainless-steel plate of 5mm width, 45mm length and 0.05mm thick was also boiled in the nanofluids for 5 min at a heat flux of 500Kw/m^2. Some irregular porous structures on the plates were observed by the authors. They mentioned that the microlayer evaporation with subsequent settlement of nanoparticles could be the reason for this formation. They observed a decrease in static contact angle from 70° to 22° and they specified that this enhancement of surface wettability is due to an increase of adhesion tension and an increase in surface roughness.

Pool boiling heat transfer characteristics of nanofluids at various pressure conditions was investigated by Liu et al [31]. They used a copper block with micro grooves as the heater surface. After boiling of CuO/water nanofluids, they observed a very thin,

smooth, block coating layer on the heater. This porous layer is believed to be steady at sub atmospheric pressures. During boiling of nanofluids, they observed an increase in both heat transfer coefficient and the critical heat flux when compared to water The authors reported an enhancement of 25%, 100% and 150% at atmospheric, 20 KPa and 7.4 KPa respectively. They reported a 50% enhancement in CHF at atmospheric pressure and 200% enhancement in CHF at a pressure of 7.4 KPa.

Coursey& Kim [32] dispersed alumina nanoparticles in ethanol and water at a concentration range of 0.001-10.02 g/L and 0.026-1.02 g/L respectively. They conducted pool boiling experiments using glass, oxidized and unoxidized copper surfaces. They observed a decrease in CHF by 22% and 13% during boiling of nanofluids on oxidized and unoxidized surfaces respectively. However, they observed that during boiling of alumina-water nanofluid at 0.525 g/L on unoxidized surface increased the CHF up to 37% when compared to water.

Liu & Liao [33] conducted pool boiling experiments by suspending CuO, SiO_2 nanoparticles in water and alcohol. During boiling of CuO/water at 0.5 wt%, they observed 27% increase in CHF and no change in boiling heat transfer coefficient when compared to water. However, SiO2 nanoparticles when suspended in water at the same concentration degraded the boiling heat transfer but increased CHF by 18% when compared to water. They reported that a sorption layer of nanoparticles was observed and prevented blanketing of vapor from easily occurring and could be the reason for the enhancement of CHF. They observed the same layer when CuO and SiO_2 nanoparticles were suspended in alcohol. In the case of alcohol based nano suspensions, they observed 31% increase in CHF with CuO particles and 20% increase with SiO_2 particles when compared to water Unsteady boiling

curves were reported by them when SDBS surfactant was mixed in water based nanofluids at 0.5 wt.%. They stated that the formation of agglutination layer was the reason for this unsteadiness in the boiling curves. In the case of alcohol based nanofluids, this surfactant addition did not form any agglutination layer of SDBS and nanoparticles.

Golubovic et al [34] observed a thin layer of nanoparticles deposited on the surface after boiling with water based nanofluids. Alumina oxide and Bismuth oxide nanoparticles were dispersed in water at concentrations up to 0.01 g/L. When compared to water, they observed an increase in CHF with nanofluids. They reported that the alumina oxide/water nanofluid increased the CHF up to 50% and the bismuth oxide/water nanofluid enhanced the CHF up to 33% when compared water. Before boiling, they observed the contact angle of a droplet of water on the clean heater to be 90º. After boiling with Al_2O_3/water nanofluid at 0.002 g/L and 0.006 g/L, they observed lower contact angles of 46.5º and 33º respectively.

Copper nanoparticles dispersed in water from 0.25 wt.% to 1.0 wt.% were used by Kathiravan et al [35] to conduct pool boiling experiments on a horizontal stainless steel tube. They stated that the copper nanoparticles when dispersed in water at 1.0 wt%, enhanced the CHF by 50% when compared to water. Boiling heat transfer coefficient was observed to be reduced at higher heat fluxes. They reported a smooth block coating on the heater surface after boiling with nanofluids and the thickness of the coating increased with concentration of nanofluid.

Park et al [36] conducted experiments using carbon nano tubes suspended in water with PVP polymer as the dispersant. The concentration of the nanofluid ranged from 0.0001 vol% to 0.05 vol%. Nanoparticles were observed to be deposited on the heater

surface after boiling. When compared to water, the boiling heat transfer coefficients of nanofluids were decreased up to 38.2% depending on the concentration of nanofluid. However, the CHF was found to be increased by 168%, 200%, 150% & 60.7% for nanofluids with 0.0001%, 0.001%, 0.01% & 0.05% concentrations respectively. Liu et al [37] conducted pool boiling experiments using CNT suspensions at various pressures. Carbon nanotubes were suspended in water at a concentration range of 0.5 wt% to 4 wt%. At atmospheric pressure, the heat transfer coefficient during boiling of 2 wt% nanofluid is 60% more than that of water and at a pressure of 7.4 KPa, the HTC is increased by 130%. The authors reported that the 2 wt% nanofluid also enhanced CHF by 63% at atmospheric pressure and by 200% at 7.4 KPa.

Kwark et al [38] studied the pool boiling characteristics of low concentration Al_2O_3/water nanofluids ($\leq$ 1g/L). Compared to water, the CHF of nanofluids increased with concentration. For the 0.0025g/L nanofluid, the CHF was approximately 80% more. They observed nanoparticle deposition on the copper heating surface after boiling. They compared the degree of nanoparticle deposition by gravity, natural convection, electric field and boiling. They revealed that the boiling process has more effect on deposition thickness.

Kole & Dey [39] investigated the pool boiling heat transfer and CHF of the ZnO/ethylene glycol nanofluids at concentrations from 0.35 vol% to 2.6 vol%. During pool boiling of 1.6 vol% nanofluid, they observed a 22% enhancement in HTC on the copper cylinder. CHF studies were performed by them using an uncoated constantan wire. They observed deposition of nanoparticles on the surface after boiling and reported an enhancement in CHF of about 117% for 2.6 vol% nanofluid. Sarafraz et al [40] observed

enhancement in both HTC and CHF by using synthesized zirconia nanofluids. A binary mixture of water and ethylene glycol mixed in equal proportions was used as the base fluid.

ZrO_2 nanoparticles were dispersed in water ethylene glycol solution at various concentrations from 0.025 wt% to 0.1 wt%. When compared to the base fluid, the 0.1 wt% nanofluid enhanced the heat transfer coefficient by 12.1% and CHF was found to be increased up to 29%. They observed nanoparticles on the heating surface after boiling. The deposited nanoparticle structures changed with respect to the concentration of the nanofluid. Huang et al [41] immersed the Ni-Cr wire in TiO_2/water nanofluid and electrically heated the wire to coat it with nanoparticles. They formed different coatings by immersing the wires in the nanofluid at a concentration range of 0.01 wt% to 1.0 wt%. When compared to bare wire, the HTC of the coated wire deteriorated with increase in nanofluid concentration. However, the CHF during boiling of 1.0 wt% nanofluid was found to be 1.7 times higher than that of water. Song et al [42] conducted pool boiling experiments with stainless steel 304 plates as test heaters. They used two plates with different surface areas. SiC nanoparticles were dispersed in water at concentrations from 0.0001% to 0.01% by volume. They observed deposition of nanoparticles on the heaters after boiling with nanofluids. For the plate with smaller surface area, they observed an increase in CHF by 39.6%, 36% & 53.5% for nanofluid concentrations of 0.0001%, 0.001% & 0.01% respectively. In the case of larger surface area plate, the 0.001% nanofluid did not enhance/deteriorate the CHF when compared to water. However, during boiling of nanofluids at 0.0001 Vol% & 0.01 Vol% concentrations, the CHF when compared to water, was enhanced by 36.2% & 105% respectively. Kamatchi et al [43] synthesized reduced graphene oxide nanoparticles and dispersed them in water at 0.01, 0.1 & 0.3 g/L. They

observed a porous layer accumulation on the Ni-Cr heater wire after boiling with rGO/water nanofluid. They stated that the thickness of the porous layer varied with the nanofluid concentration. When compared to water, the CHF was enhanced by 145%, 180% & 245% during pool boiling of rGO/water nanofluid at 0.01, 0.1 & 0.3 g/L concentrations respectively.

Unlike the above studies, Kathiravan et al [44] & Diao et al [45] reported deterioration in CHF during pool boiling of nanofluids. Kathiravan et al [44] dispersed the carbon nanotubes in water at 0.25 vol%, 0.5 vol% and 1.0 vol% with and without SDS surfactant. At a heat flux of 500 KW/m^2, the HTC during pool boiling of CNT/water nanofluid at 0.25 vol%-1.0 vol% was found to be 1.5-, 2.6- & 3.0 times more than that of water. However, the CHF during boiling of nanofluids was found to be less than that of water irrespective of surfactant addition. Diao et al [45] conducted pool boiling experiments by dispersing copper nanoparticles in R141-b at 0.008 vol%, 0.015 vol% & 0.05 vol%. They added SDBS to stabilize the Cu-R141b nano refrigerant. They observed an enhancement in the heat transfer with the nano refrigerants, but the CHF was found to be deteriorated when compared to pure R141-b.

In summary, the nanoparticle deposition on the heater surface causes activation of new nucleation sites, thereby increasing the rate of heat transfer. If the heater surface is smooth, then the deposition could further smoothen the surface and deteriorate the heat transfer. Most of the studies reported that the nanoparticle layer formed during boiling, alter the surface conditions, and hence could delay the CHF. However, there is no clear agreement on whether pool boiling of nanofluids can enhance/deteriorate the rate of heat transfer.

CHAPTER III. EXPERIMENTAL APPARATUS

The bubble parameters during pool boiling of nanofluids, were measured using the experimental apparatus as shown in Fig 2. The test facility consists of:

1. DC power supply
2. Data Acquisition system (DAQ)
3. Computer
4. High-speed camera
5. Boiling chamber
6. Pool cartridge heaters
7. Variable transformer
8. Copper-Teflon assembly

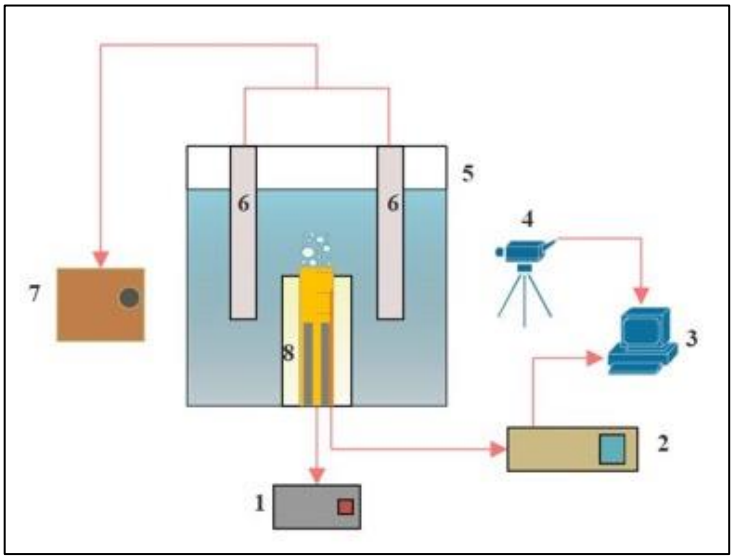

Figure 2: Schematic of pool boiling facility

Boiling Chamber

A chamber with 152.4 mm sides was constructed by welding five stainless steel plates of 3.175 mm thickness. A larger container which is 203.2 mm in height and 228.6 mm in length was constructed by welding five mild steel plates of 6.35 mm thickness. Through holes of 88.9 mm diameter were drilled on the side walls of both the chambers. As seen in Fig.3, the stainless-steel chamber was enclosed inside the larger mild steel structure by welding stainless steel pipes in between the chamber walls. The clearance between the chambers was packed with insulating wool to prevent loss of heat during boiling.

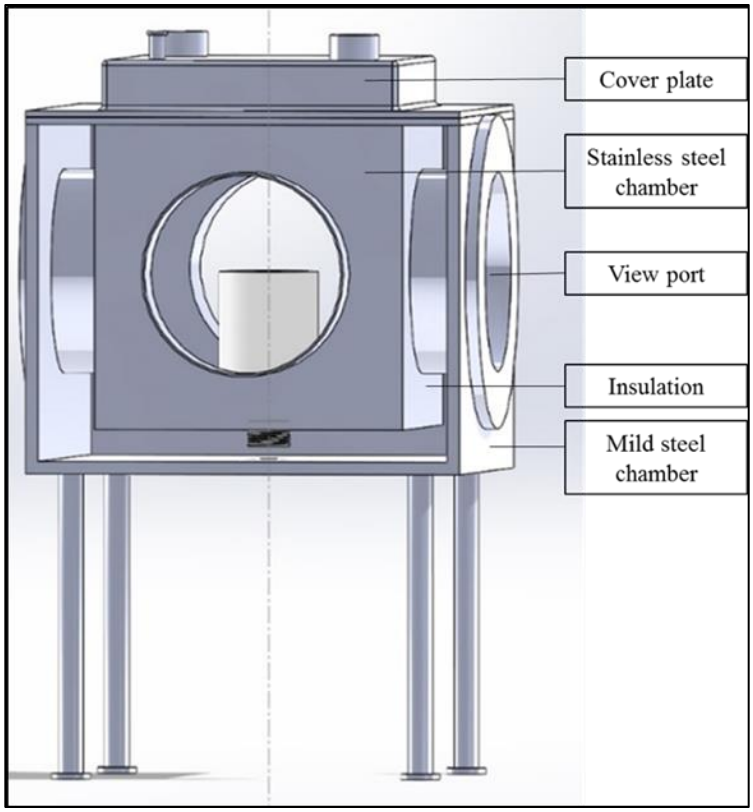

Figure 3 Boiling Chamber

The disc shaped Pyrex glasses were mounted to the grooves on the mild steel chamber. These glasses on the side walls were secured in place by bolting a 101.6 mm

diameter flange to the tank body. Silicone gaskets were used to make the view ports leak proof. A threaded pipe was welded at the center of the bottom plate to screw the copper-Teflon assembly. The chamber was covered by a stainless-steel plate packed with insulating wool. The cover plate has holes drilled to insert the two pool cartridge heaters, each with a maximum power of 350W. The power supplied to the pool heaters was controlled by using a variable transformer. A K-type thermocouple is inserted into the pool, through a hole on the top cover plate. A vent on the top plate maintains the pool at atmospheric pressure.

Copper-Teflon Assembly

The top of a copper cylinder, which is 12.70 mm in diameter and 63.50 mm in length was chosen as the heating surface. Four cartridge heaters, which are 3.17 mm in diameter and 38.10 mm in length were press fitted to the copper cylinder from the bottom. Each heater can provide up to 60 W of power. The material of the cylinder is made out of oxygen free high thermal conductive copper to ensure that maximum amount of heat generated by the cartridge heaters is transmitted across the length. The temperatures across the length of the copper rod were obtained by three K-type thermocouples. The thermocouple wires were inserted into the center of copper rod through the machined holes which are 0.50 mm in diameter. The first thermocouple is located at 1 mm from top of the surface. The second and third thermocouples are located at 10 mm and 20 mm from the first thermocouple respectively. The dimensions of the copper cylinder and thermocouple locations are as shown in Fig 4.

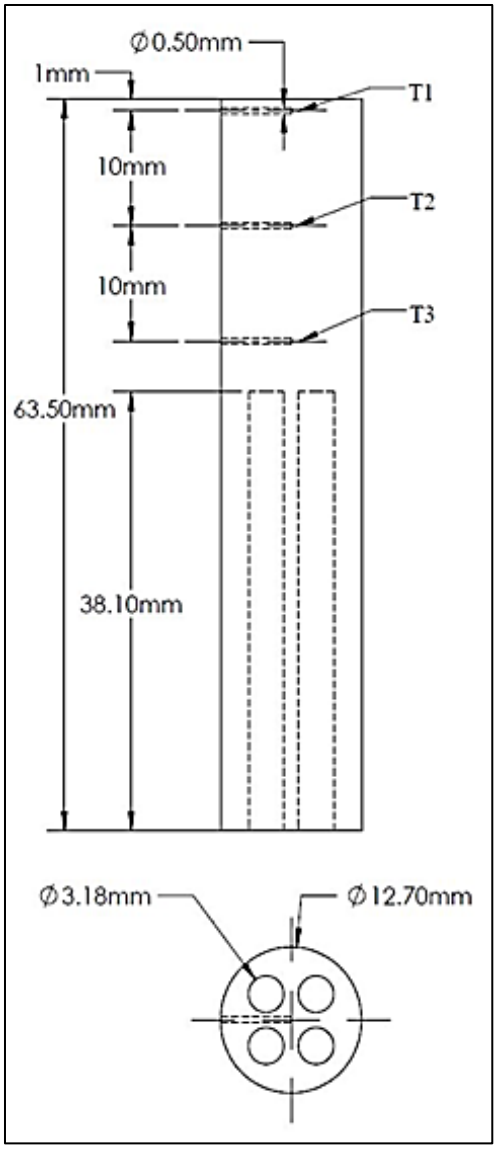

Figure 4 Geometry of copper rod

For accurate temperature measurements, high thermal conductive cement was used to pot the thermocouple beads.

In order to prevent heat loss from the copper cylinder, a Teflon tube was machined as an outer sleeve. The outer diameter of the Teflon tube is 50.80 mm and the length is 75.20 mm. The copper cylinder was enclosed in the Teflon tube by using an insulating epoxy as shown in Fig 5.

The thermocouple and heater wires were first passed through the hole at the chamber base and then the copper-Teflon assembly was screwed to the base.

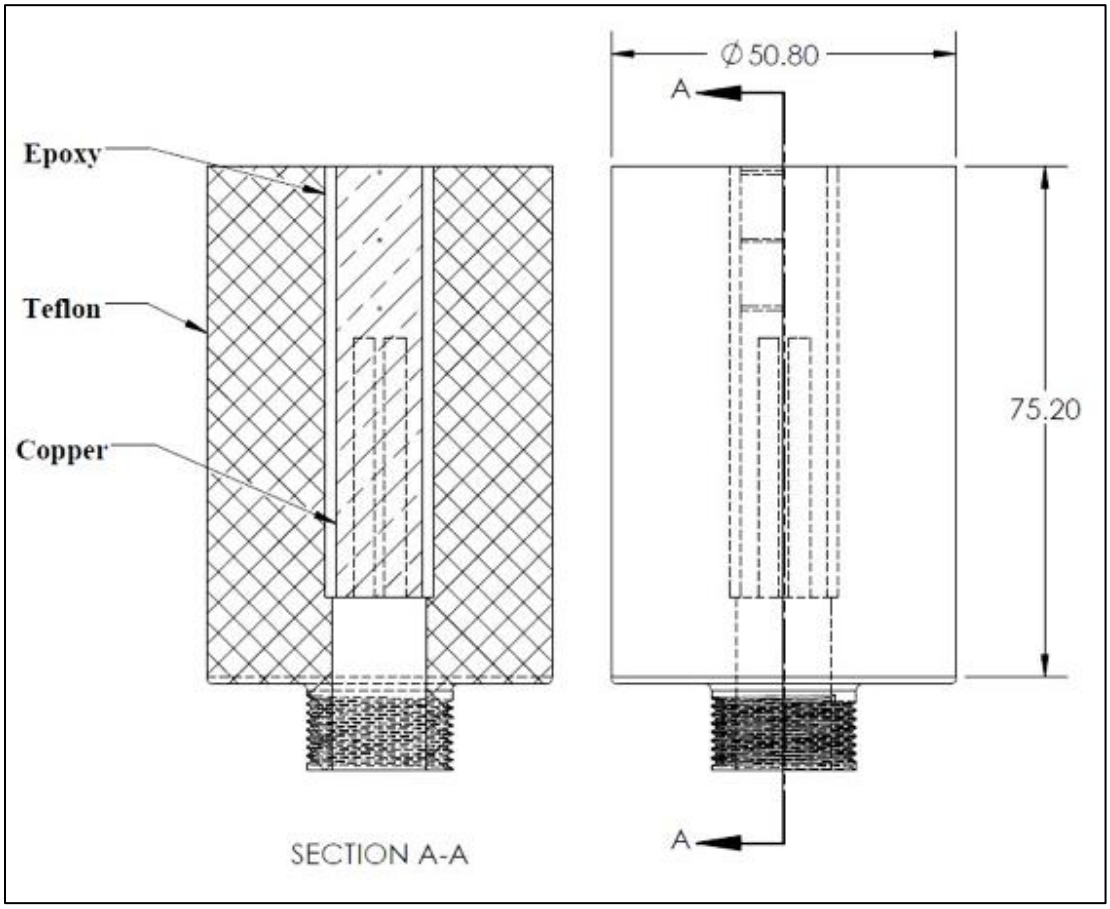

Figure 5 Copper-Teflon assembly

The press fitted cartridge heaters were connected in parallel and powered by BK precision 9206 DC power supply. The applied power to the heaters was controlled via a computer to which the DC power supply was connected. The software provided by the manufacturer was used to record the power input to the heaters at a rate of 1 sample per second.

The K-type thermocouple lead wires were welded to form a bead. The size of the bead is kept to the smallest for improved response rate. Prior to installation, three-point

calibration of thermocouples was performed at ice, room and boiling temperature points. All the thermocouple readings were adjusted by using the calibration results.

Data Acquisition System

The measurements were recorded using a National Instruments cDAQ-9174 data acquisition system. A NI-9213 thermocouple module which has 16 thermocouple channels was connected to the data acquisition system. All the thermocouples from the test section and the boiling chamber were connected to this module using thermocouple extension wires. The data was obtained at 1 Hz sampling rate per channel in high resolution mode. The thermocouple module has a cold-junction compensation accuracy of 0.8° C. A LabView signal express interface displays the instantaneous temperature readings from all the thermocouples, while simultaneously recording the measurements to a Microsoft Excel file.

High Speed Video Camera

A Fastec Imaging IL5 camera fitted with Infinity KX infinimax long distance microscope captured the entire boiling process. The microscopic lens was equipped with Infinity MX-4 objective to get a closer look at the bubble growth during pool boiling. The camera settings were adjusted by using FasMotion software. A 500 W halogen lamp provided the required lighting for recording videos. The photograph of the setup is as shown in Fig.6. The obtained videos were processed by using ImageJ software to analyze the bubbles by each frame.

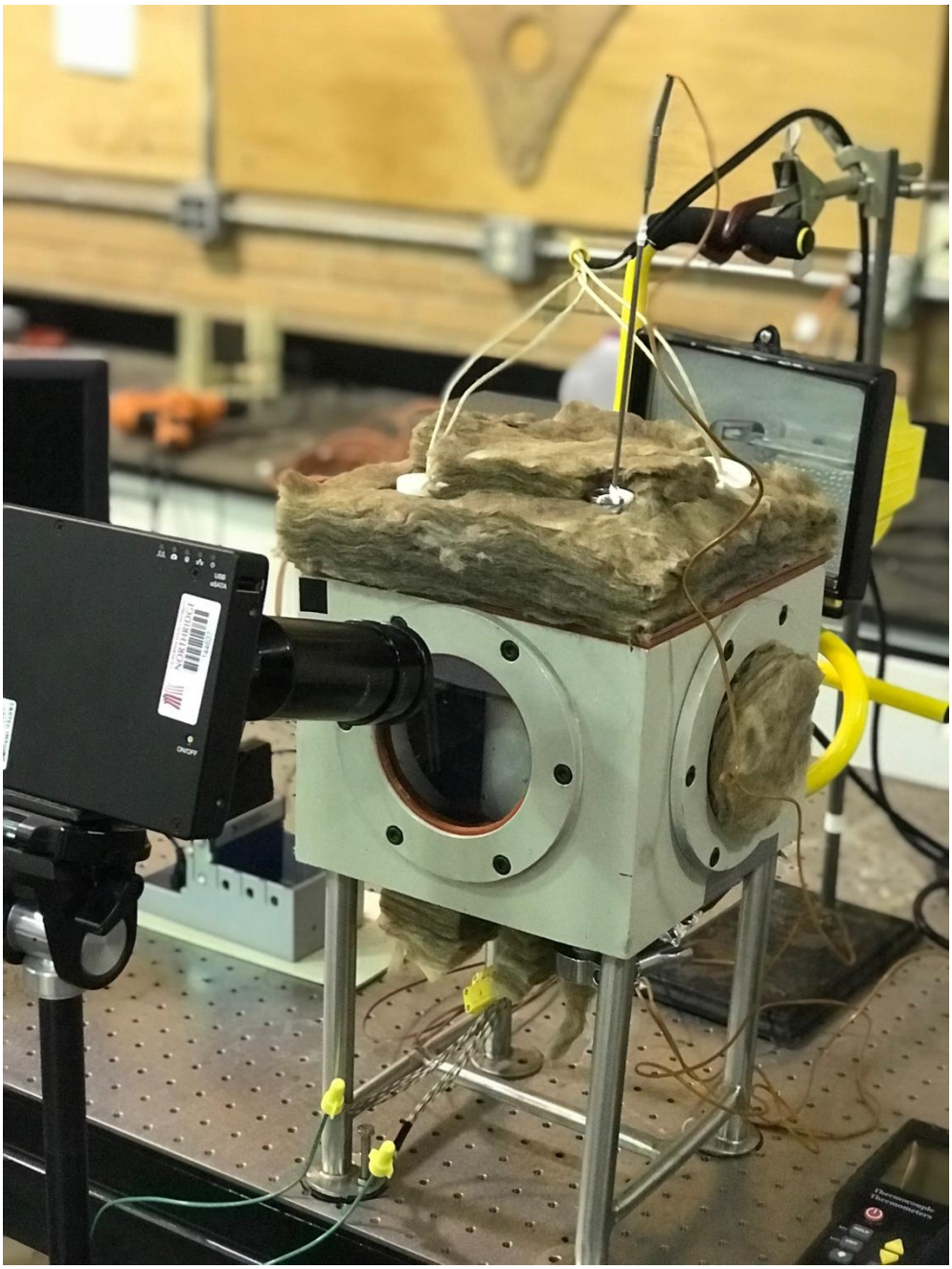

Figure 6 Photograph of experimental apparatus showing high speed camera

CHAPTER IV. EXPERIMENTAL PROCEDURE

Pool boiling experiments were conducted using Al_2O_3/water nanofluids, containing alumina nanoparticles of sizes 10 nm & 30 nm. The Al_2O_3 nanoparticles aqueous dispersions at a concentration of 20 wt% were purchased from US Research Nanomaterials, Inc.

Nanofluid Preparation

The procured nanofluids of both particle sizes are translucent liquid-white in appearance. The gamma crystal structured Al_2O_3 nano particles are 99.99% in purity. According to the manufacturer, the PH value of the concentrated solution is greater than 7. The 20 wt% concentrated nano dispersions supplied in weight concentration ω is converted to volume concentration ϕ, by using Eq. (4).

$$\phi = \frac{\omega \rho_w}{\left(1 - \frac{\omega}{100}\right)\rho_p + \frac{\omega}{100}\rho_w} \tag{4}$$

Where, ρ_w is the density of water and ρ_p is the density of nanoparticles.

Both the stock nanofluids were diluted to the required concentrations of 0.001% and 0.0001% by volume using distilled water. About 3.8 liters of diluted nanofluids at each concentration were prepared prior to the experiment. The volume of stock nanofluid to be added for each required concentration is calculated using Eq. (5).

$$V_1 = \frac{V_2 \emptyset_2}{\emptyset_1} \tag{5}$$

Where, V_1 & $\emptyset_1$ are the volume and concentration of stock solution, V_2 & $\emptyset_2$ are the required volume and concentration of nanofluid. The diluted nanofluid was stirred for 45 min just before the experiment using an overhead stirrer for proper dispersion of nanoparticles.

Copper Surface Cleaning

Prior to each experiment, extra care was taken to clean the boiling chamber and the copper surface to remove any deposited nanoparticles. They were rinsed thoroughly by using distilled water. After drying, the copper surface was cleaned using isopropyl alcohol. The copper surface was washed again using distilled water to remove any residual layer of chemicals.

Degassing of Test Liquid

The test liquid (distilled water or nanofluid) was then added to the boiling chamber and the pool cartridge heaters were powered to boil the liquid vigorously for 45-60 min. This procedure removes any dissolved non-condensable gases from the liquid.

Nucleation of Bubbles

After the degassing procedure, the test liquid was heated up to saturation temperature. Once the pool reaches steady state, the cartridge heaters inserted into the copper rod were switched on. The applied power was increased gradually by changing the applied voltage to the cartridge heaters. After some time, nucleation is visible on the copper surface. The pool cartridge heaters were switched off to allow the liquid to come to rest and videos of bubbles were taken. At each voltage increment, the copper surface was allowed to reach steady state before obtaining the required data.

Data Collection

At each applied power, the bubbles nucleating on the copper surface were captured by the high-speed camera at 558 FPS. A total of 2353 frames were recorded with a time interval of 1.79221 ms between each frame. The pool cartridge heaters were switched on when required to maintain the pool at saturation temperature. The obtained videos at each superheat temperature were converted to jpeg images for measuring the bubble parameters. The temperature, voltage and current readings were recorded at steady state of each power input. The thermocouple readings were recorded at 1 Hz for 180 seconds, while voltage and current readings were recorded continuously at 1 sample/s.

Data Analysis and uncertainty

The Teflon tube around the copper rod reduces the radial heat losses. As seen in Fig.7, the temperatures along the length of the copper cylinder at various applied heat fluxes are linear. Hence it is assumed that the heat is being conducted in axial direction along the length of the copper rod.

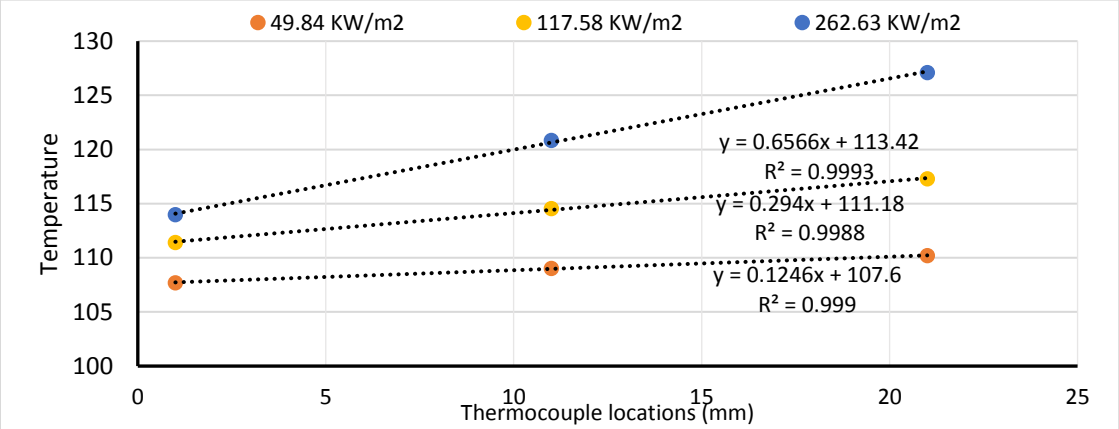

Figure 7 Temperature profiles along the length of the copper rod at various applied heat fluxes

The heat flux (q″) at each power input is calculated using the 1-D conduction equation.

$$q'' = -k_{cu}\frac{dT}{dx} \tag{6}$$

where k_{cu} is the thermal conductivity of the copper. The temperature gradient $\frac{dT}{dx}$ is evaluated by using Eq.7.

$$\frac{dT}{dx} = \frac{T_1 - T_3}{2.x_1} \tag{7}$$

The wall temperature T_w is estimated using Eq.8,

$$T_w = T_2 - \frac{x_2.q''}{k_{cu}} \tag{8}$$

Where $x_1 = 10\ mm$, $x_2 = 11\ mm$ and T_1, T_2 & T_3 are the temperature readings along the copper rod. The schematic of the copper rod with thermocouple locations is as shown in Fig.8.

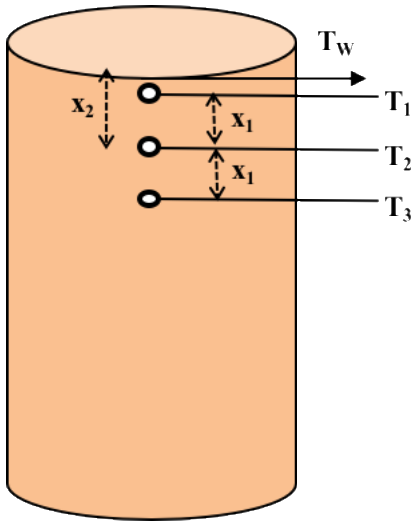

Figure 8 Schematic of the thermocouple locations

While measuring the bubble parameters, the processed images are calibrated to a reference image taken during each experiment. A thermocouple of known dimension is used for the reference picture. The bubble equivalent diameter is defined as the diameter of sphere with equal volume of spheroidal bubble. Eq.9 is used to calculate the equivalent diameters of bubbles. Fig.9 illustrates the measurements made on a typical bubble on the copper heater.

$$D_{eq} = \sqrt[3]{B^2 C} \tag{9}$$

where B and C are the measured horizontal and vertical diameters of a bubble.

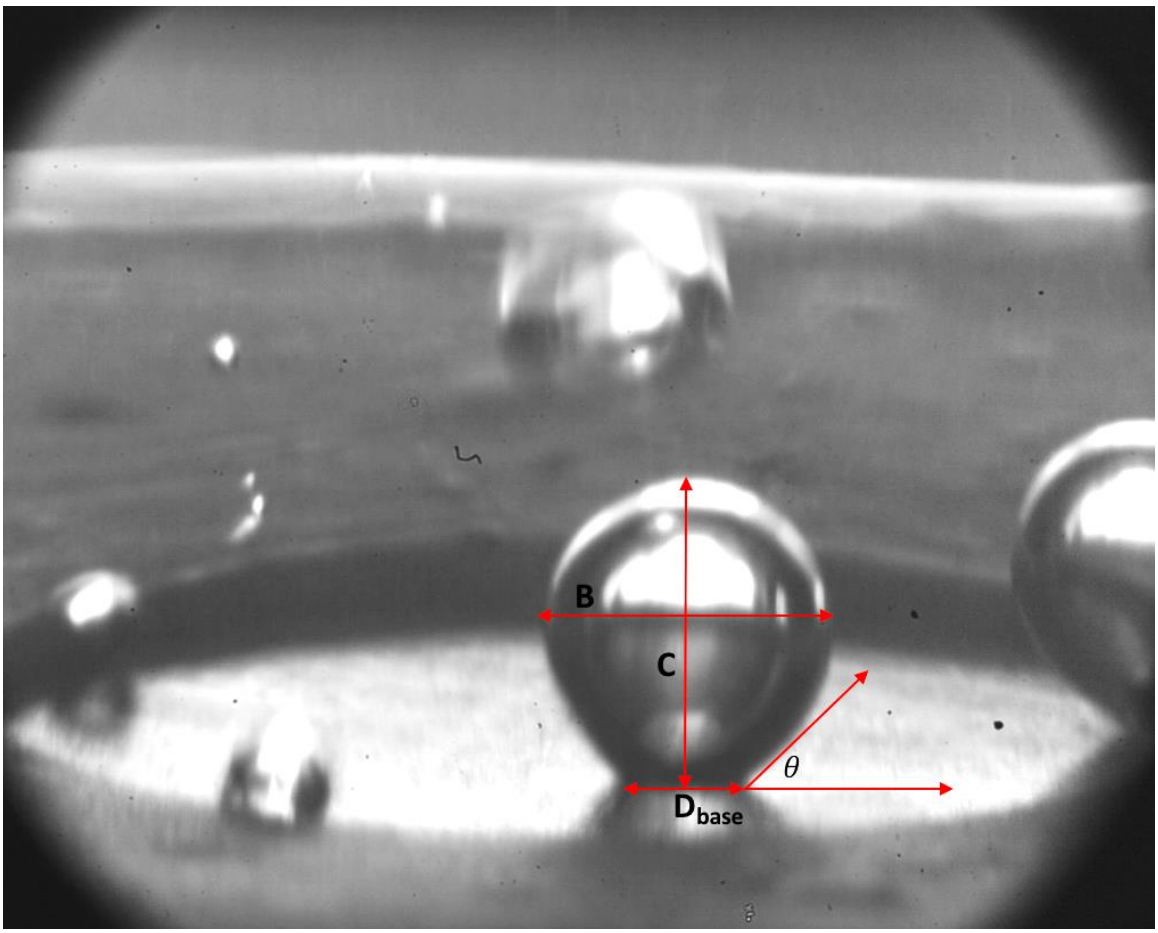

Figure 9 Sample image of a bubble showing typical measurements

In this study, the uncertainties can originate from thermocouple calibration accuracy and precision, thermal conductivity of copper and length measurements. During calibration of the thermocouples, the precision error was evaluated at steady state temperatures by calculating twice the standard deviation to obtain 95% confidence interval. The uncertainty in calculation of heat flux and wall temperature is determined as:

$$\frac{\mathrm{U}_{\frac{dT}{dx}}}{\frac{dT}{dx}} = \sqrt{\left(\frac{U_{T_1}}{T_1 - T_3}\right)^2 + \left(\frac{U_{T_3}}{T_1 - T_3}\right)^2 + \left(\frac{U_{x_1}^2}{x_1}\right)^2} \tag{10}$$

$$\frac{\mathrm{U}_{q"}}{q"} = \sqrt{\left(\frac{U_{k_{cu}}}{k_{cu}}\right)^2 + \left(\frac{\mathrm{U}_{\frac{dT}{dx}}}{\frac{dT}{dx}}\right)^2} \tag{11}$$

$$\frac{U_{T_w}}{T_w} = \sqrt{\left(\frac{U_{T_2}}{T_w}\right)^2 + \left(\frac{\mathrm{U}_{q"}x_2}{T_w k_{cu}}\right)^2 + \left(\frac{U_{x_2}q"}{T_w k_{cu}}\right)^2 + \left(\frac{U_{k_{cu}}q"x_2}{T_w {k_{cu}}^2}\right)^2} \tag{12}$$

The uncertainties of the parameters used in this study are as shown in Table.1.

Table 1 Uncertainties of parameters

U_P	**Value**	**Units**
U_{T_1}	0.32	°C
U_{T_2}	0.25	°C
U_{T_3}	0.25	°C
U_{x_1}, U_{x_2}	0.0001	m
$U_{k_{cu}}$	9	W/m-K

CHAPTER V. RESULTS AND DISCUSSION

The obtained data during pool boiling of water is compared with the well-known Rohsenow correlation to validate the accuracy of the test setup. The Rohsenow correlation is written as:

$$q'' = \mu_f h_{fg} \left[\frac{g(\rho_f - \rho_g)}{\sigma}\right]^{\frac{1}{2}} \left[\frac{C_{pf}\Delta T}{C_{sf} h_{fg} Pr_f{}^n}\right]^3 \quad (13)$$

Where ΔT=T_w-T_{Sat} is superheat temperature, C_{sf} and n are constants. Fig.10 compares the correlation with $C_{sf} = 0.009$ and n=1 for water, with the present experimental results.

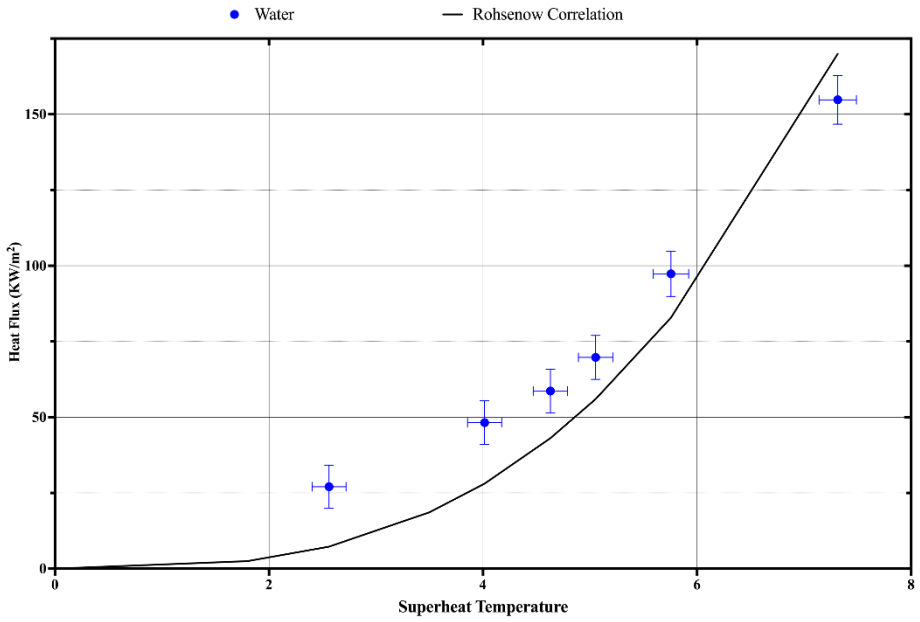

Figure 10 Validation Curve

As seen in the above figure, the correlation reasonably agrees with the present data.

In the following sections, the change in wall heat transfer due to nanofluid boiling is presented by comparing the obtained results with that of water. Then the bubble

parameters during water and nanofluid boiling are compared with respect to nanofluid concentration and particle size. Lastly, the measured bubble diameters are utilized to investigate the energy transferred per bubble due to microlayer evaporation.

Pool boiling Curves

The heat flux and superheat temperature results of nanofluids are compared with water in Fig 11. As shown in the figure, the data of nanofluids shift towards the right indicating deterioration in heat transfer. During boiling of nanofluids, the deterioration in wall heat transfer when compared to water increases with heat flux. At 50 KW/m^2, the effect of nanofluid concentration and particle size on deterioration of heat transfer is significant. However, at 100 KW/m^2 these effects on deterioration are less significant. A thin coating of nanofluid on the copper surface was noticed after pool boiling experiments with nanofluids. This may explain the increase in wall surface temperature thereby deteriorating the heat transfer.

Saeid Vafaei [46] conducted experiments using water based nanofluids containing 20-150 nm sized alumina nanoparticles at 0.001% to 0.1% concentrations by volume. Similar deterioration in heat transfer due to nanofluid boiling was observed by the author. Fig.12 compares the nanofluid data of this study with the experimental data of Saeid Vafaei [46]. As seen in the figure below, the results during boiling of 10nm sized Al_2O_3/Water at 0.001 vol% reasonably agrees with the experimental data of Saeid Vafaei [46].

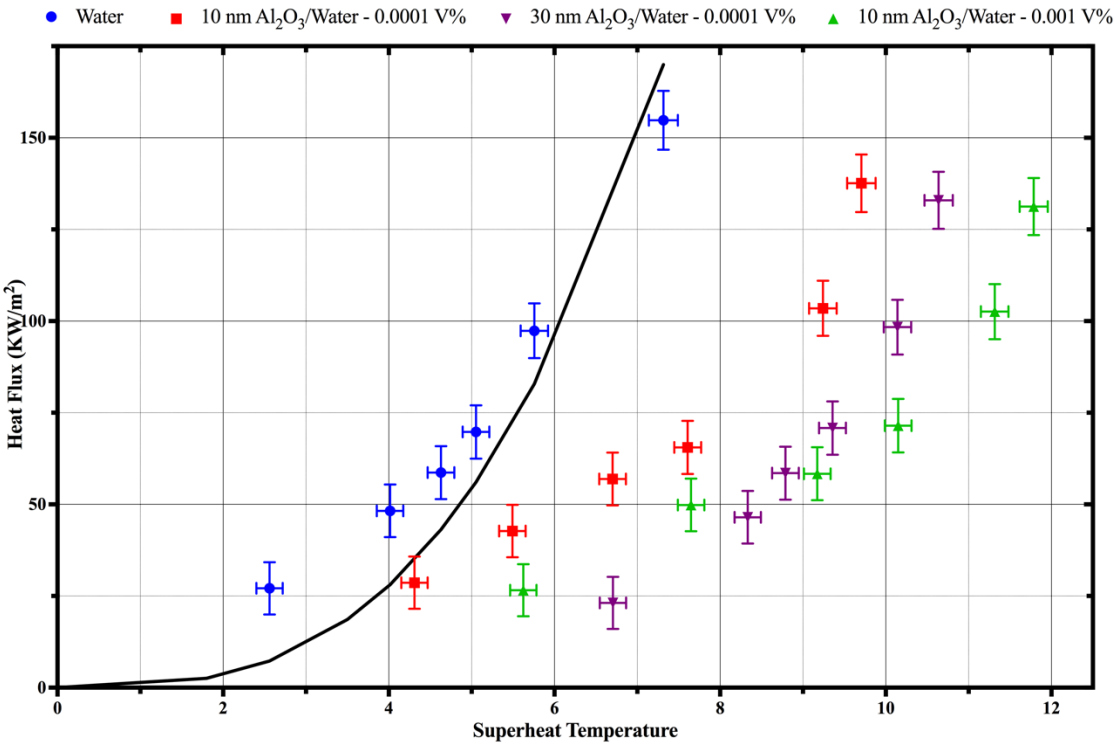

Figure 11 Pool boiling curves of water and nanofluids

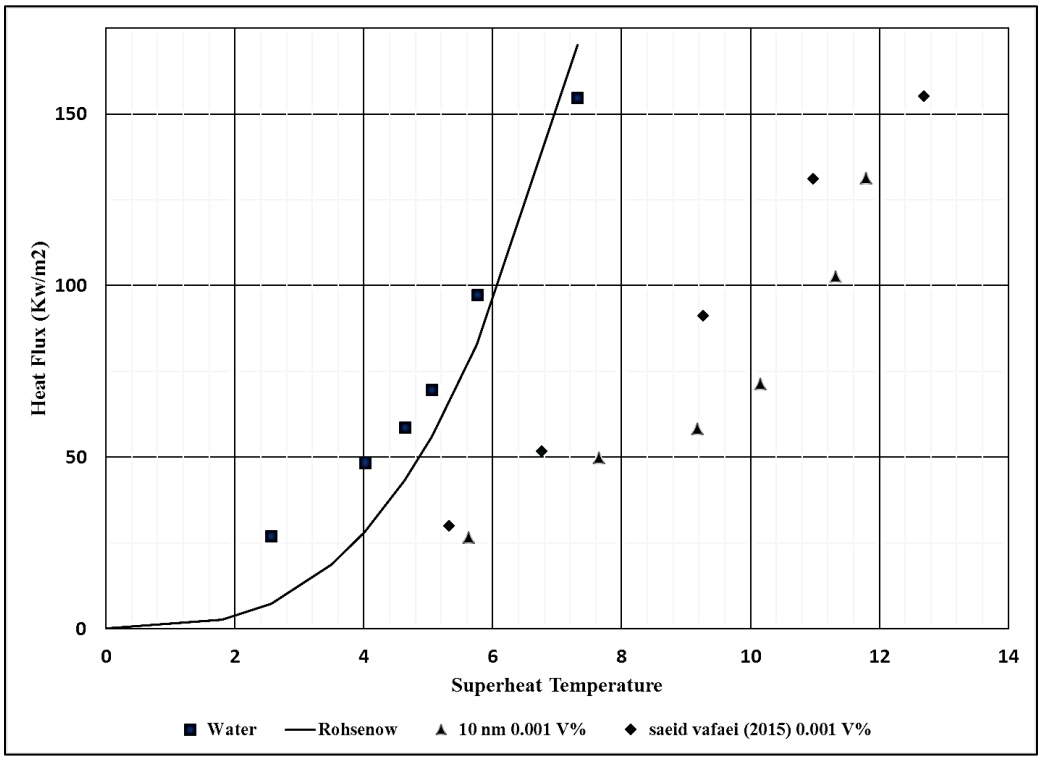

Figure 12 Comparison of present data with experimental data of Saeid Vafaei [46]

Bubble growth and departure at heat flux of 45.82 KW/m^2

The pictures of bubbles from nucleation to departure are as shown in Fig.13. During boiling of water, the bubbles begin to grow and reach their maximum diameter in 125 ms and finally depart the surface at 200 ms. During boiling of nanofluids containing 10 nm sized particles at 0.0001% and 0.001%, the total growth time of bubbles is close to 100 ms. As seen in Fig.13, the growth time of bubbles are faster in nanofluids when compared to water. The time taken to grow to their maximum size is also less. At a concentration of 0.0001%, the bubbles grow to their maximum size at 57 ms and at 0.001% the time taken by the bubbles is 91 ms.

For 0.0001% nanofluid containing 30 nm sized particles, the bubbles quickly grow to their maximum size at 9 ms and depart the surface at 14 ms. When compared to water and nanofluid containing 10 nm particles, the bubble growth and departure is significantly faster.

Due to the addition of alumina nanoparticles, both the bubble growth time and the time to reach the maximum bubble size is reduced. The rate of decrease is almost same when the concentration of nanofluid is increased from 0.0001 Vol% to 0.001 Vol%. Whereas, the rate of change is highly significant when the particle size in the nanofluid is increased from 10nm to 30nm.

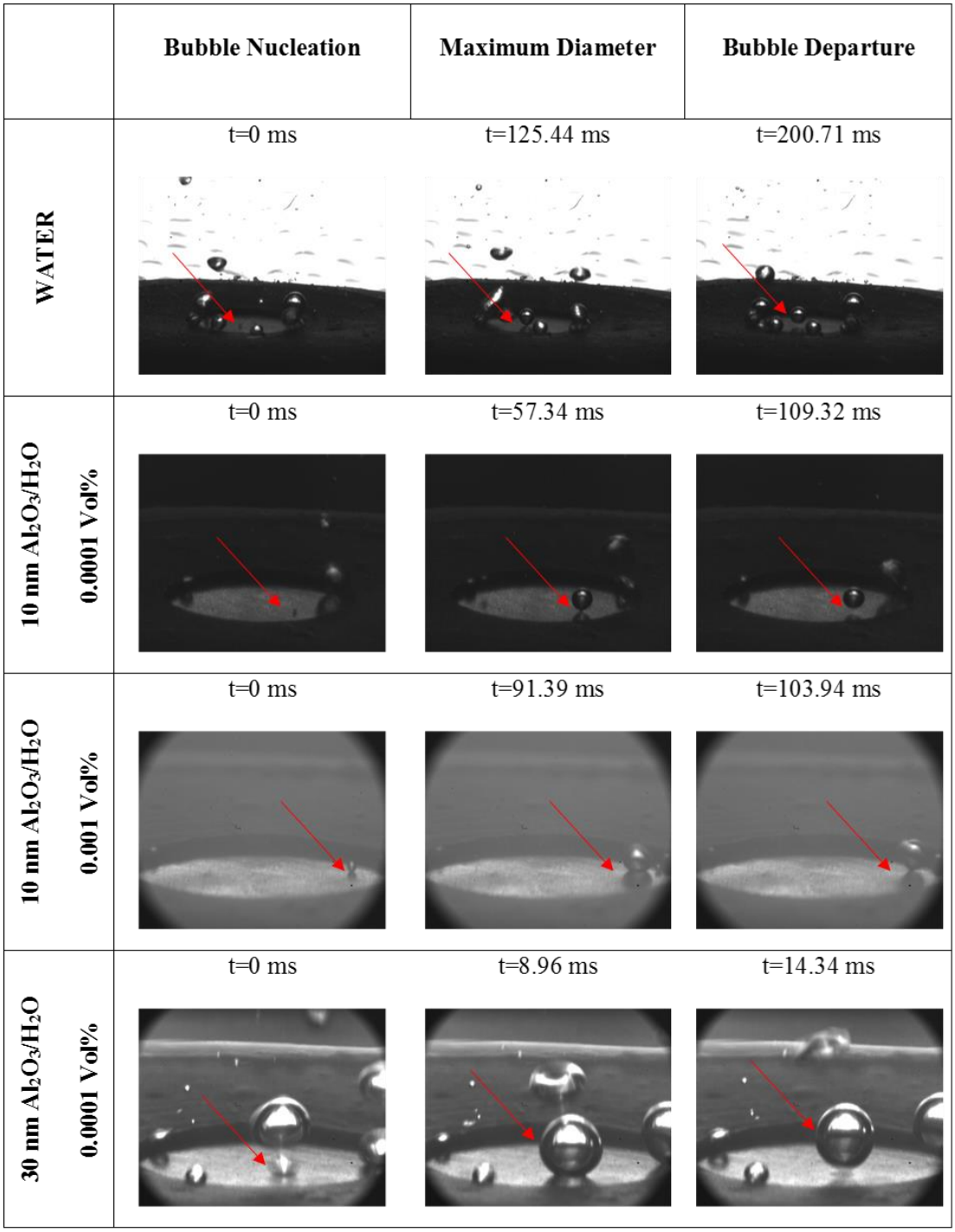

Figure 13 Growth of a bubble during boiling of water and nanofluids at 45.82 KW/m^2

The measured average bubble base diameters during boiling of water and nanofluids at 45.82 KW/m^2 are presented in Fig.14.

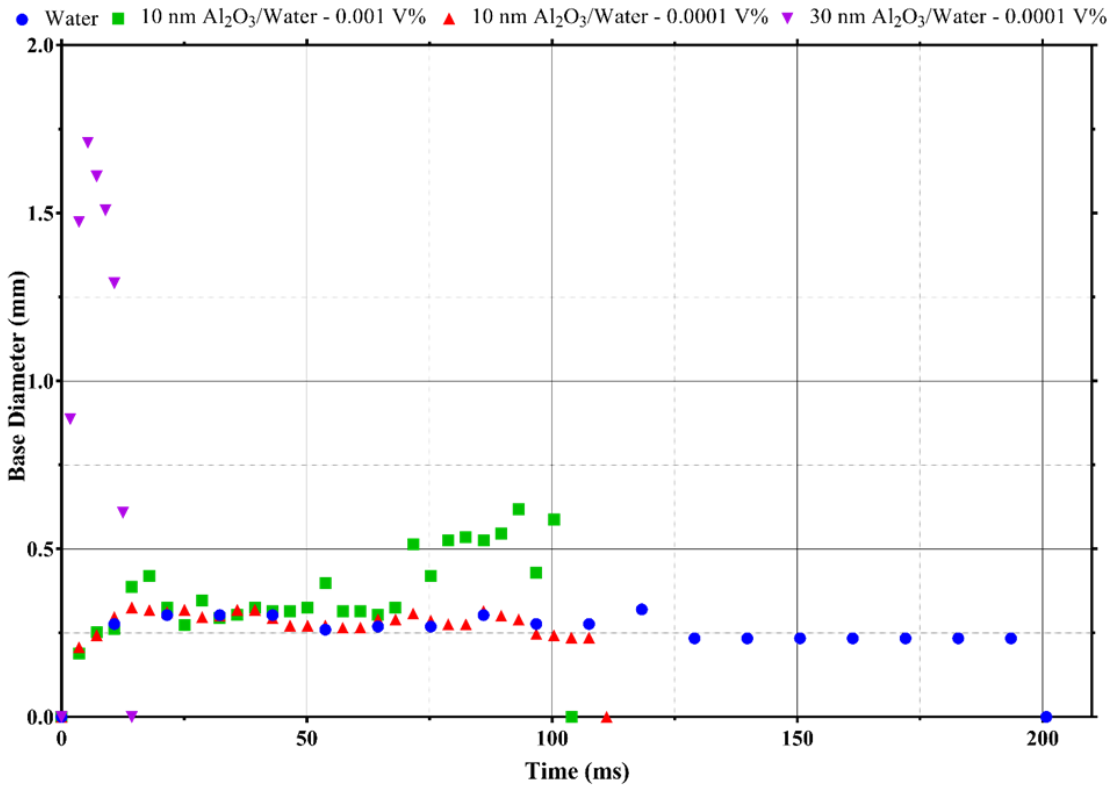

Figure 14 Comparison of bubble base diameters during boiling of nanofluids with water at 45.82 KW/m^2

During boiling of water, the base diameter of bubbles increases to a maximum of 0.32 mm. After that, the base of the bubbles remain steady for a specific time, and then they depart the surface. The bubble base growth trend is observed to be similar for the nanofluid at 0.0001% containing the particles of 10 nm size. When the concentration is increased to 0.001% the bubble base expands, and contracts frequently exhibiting a stick-slip behavior as shown in Fig.14. The maximum bubble base diameter is 0.76 mm. A significant increase in bubble base diameter is observed during boiling of nanofluid

containing 30 nm particles at 0.0001% concentration by volume. The bubbles expand quickly at the base to a maximum diameter of 1.70 mm.

The measured average bubble equivalent diameters during boiling of water and nanofluids at 45.82 KW/m^2 are as shown in figure 15.

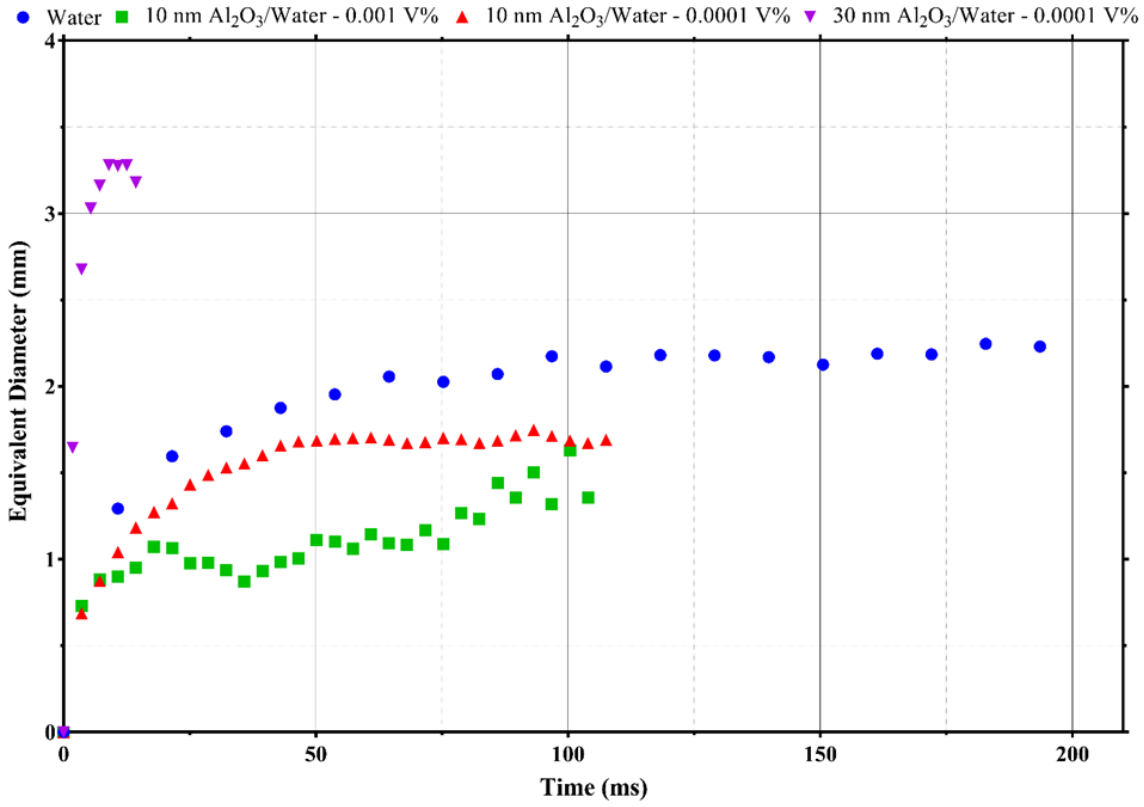

Figure 15 Comparison of bubble equivalent diameters during boiling of nanofluids with water at 45.82 KW/m^2

The bubbles formed during boiling of water grow in size to a maximum equivalent diameter of 2.26 mm. The growth trend is similar for the nanofluid at 0.0001% containing the particles of 10 nm size. However, the equivalent diameters are less when compared to that of water. The maximum equivalent diameter is about 1.75 mm. When the concentration is increased to 0.001% the bubbles begin to grow at a slower rate and the fluctuations in the bubble diameter can be seen in Fig.15, with a maximum diameter of

1.63 mm. A significant increase in size of the bubbles is observed during boiling of nanofluid containing 30 nm particles at a concentration of 0.0001 Vol%. The bubble growth rate is high as it nucleates and the maximum equivalent diameter before departure is 3.28 mm. This shows high rate of heat transfer into the bubble when 30 nm sized particles are used. It is evident that at this applied heat flux, the effect of nanofluid particle size on the bubble dynamics is more significant as compared to the nanofluid concentration.

The measured contact angles during boiling of water and nanofluids at 45.82 KW/m^2 are as shown in Fig.16. During boiling of water, the bubbles grow in size with an average receding contact angle of 27° and departs the surface with an average advancing contact angle of 36°. The bubbles formed during boiling of nanofluid containing 10 nm sized particles at 0.0001 vol%, have lower contact angles when compared to water. The average receding contact angle is 22° and the average advancing contact angle is 23°. When the concentration of the same nanofluid is increased to 0.001%, a stick-slip behavior by the bubbles is observed and is as shown in Fig.16. The average receding contact angle is 26° and the average advancing contact angle is 35°. The high nanofluid concentration is probably responsible for non-uniform deposition of the particles on the surface resulting in the stick-slip behavior of the bubble base. When the nanoparticle size is increased from 10 nm to 30 nm, the bubbles begin to grow with an average receding contact angle of 21° and departs the surface with an average advancing contact angle of 33° similar to water. The presence of high concentration of 30 nm sized particles in the liquid surrounding the bubble base is probably causing significantly higher rate of heat conduction and corresponding higher rate of evaporation into the bubbles since the contact angle is slightly lower when compared to pure water.

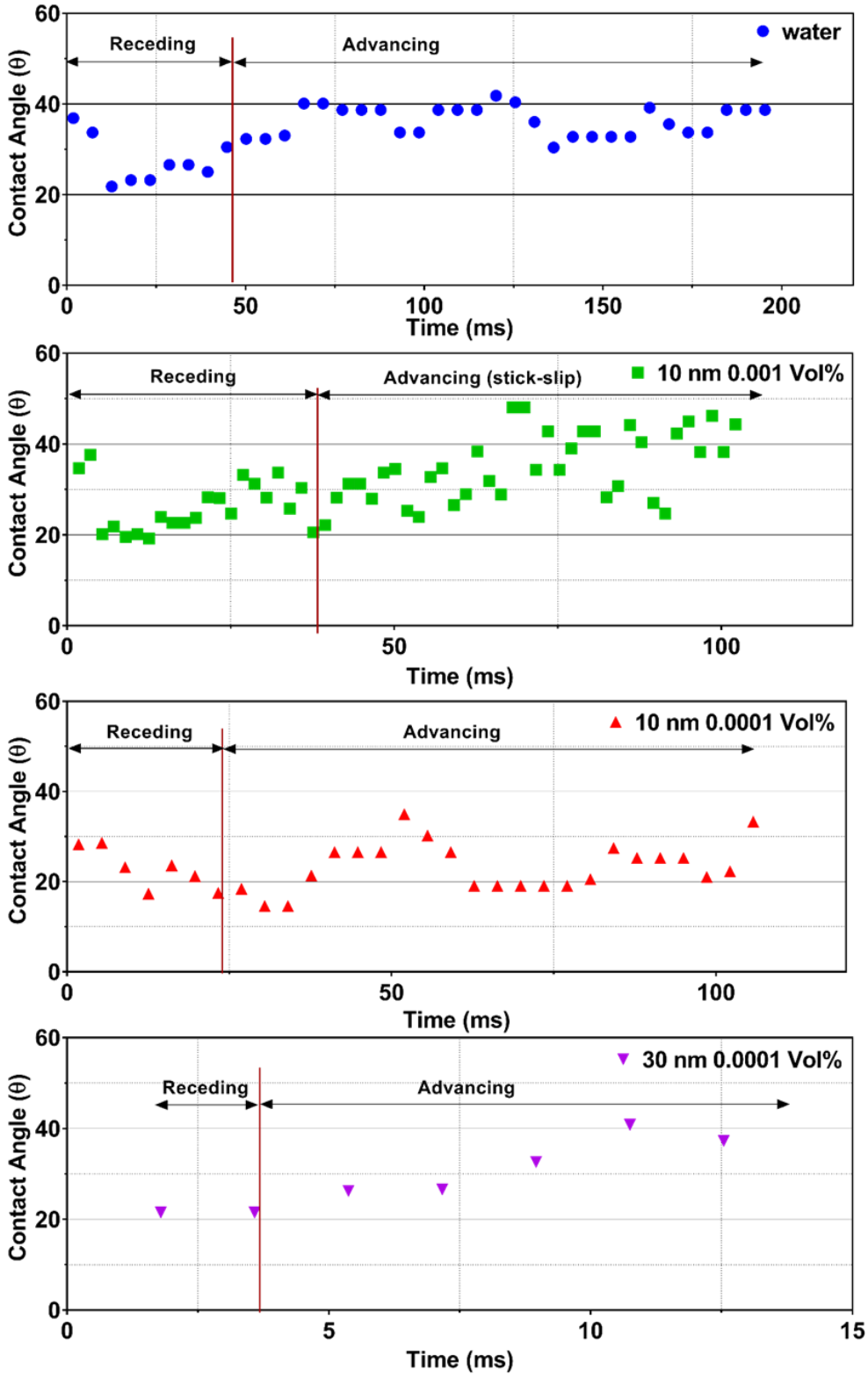

Figure 16 Comparison of bubble contact angles during boiling of nanofluids with water at 45.82 KW/m^2

Bubble growth and departure at heat flux of 65.53 KW/m^2

The pictures of bubbles from nucleation to departure are as shown in Fig.17. During boiling of water at heat flux of 65.53 KW/m^2, the bubbles begin to grow and reach their maximum diameter in 75 ms and finally depart the surface at 95 ms. During boiling of nanofluids containing 10 nm sized particles at 0.0001% and 0.001%, the total growth time of bubbles is close to 15 ms. As seen in Fig.17, the growth time of bubbles is faster in nanofluids when compared to water. The time taken to grow to their maximum size is also less. At both the concentrations, the bubbles grow to their maximum size at 11 ms.

For 0.0001% nanofluid containing 30 nm sized particles, the bubbles quickly grow to their maximum size at 11 ms and depart the surface at 16 ms. The bubble growth and departure is significantly faster when compared to water. At the heat flux of 65.53 KW/m^2, the rate of decrease in growth time of bubbles for nanofluids is same, irrespective of nanoparticle size and concentration.

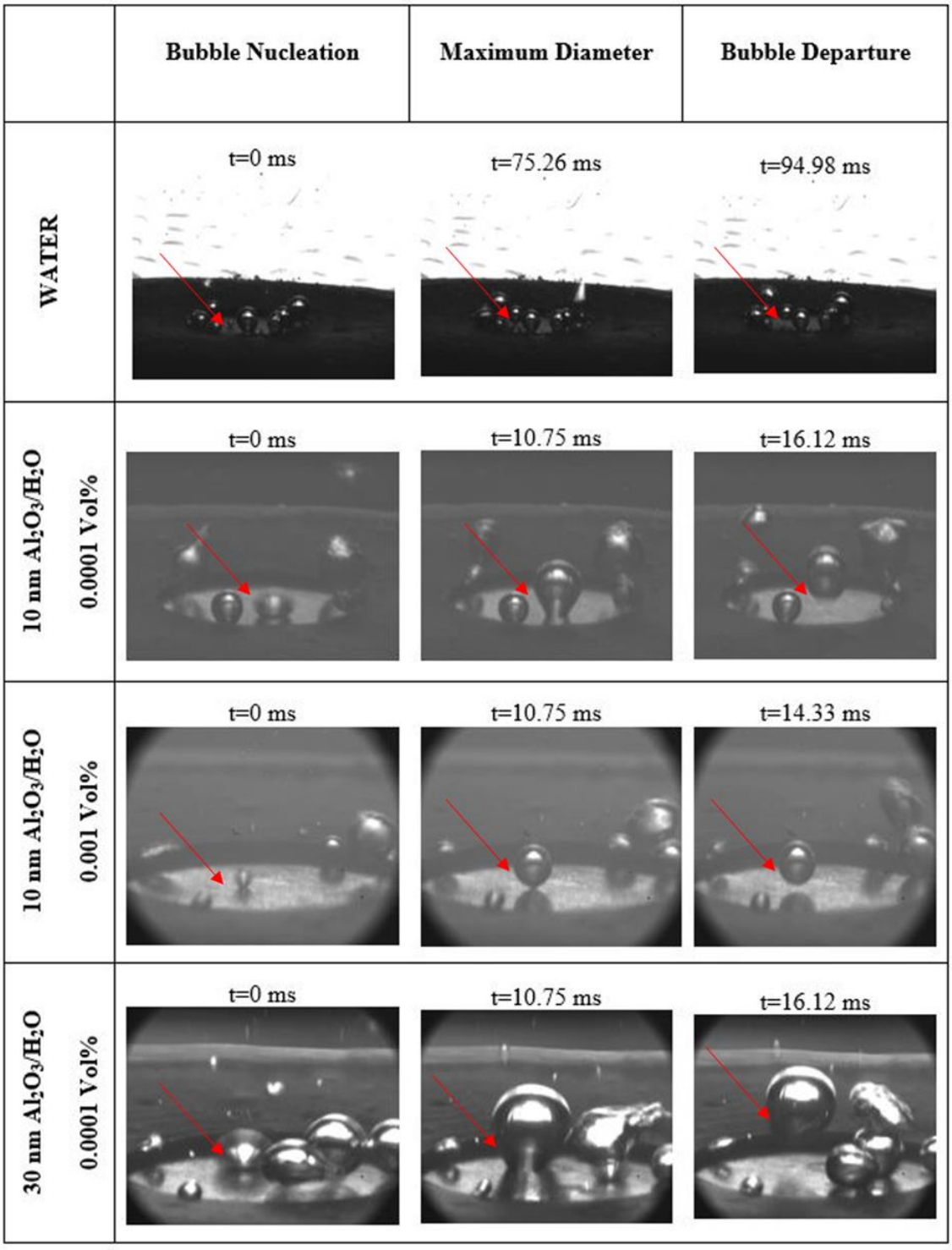

Figure 17 Growth and departure of a bubble during boiling of water and nanofluids at 65.53 KW/m^2

The measured average bubble base diameters during boiling of water and nanofluids at 65.53 KW/m^2 are presented in Fig.18.

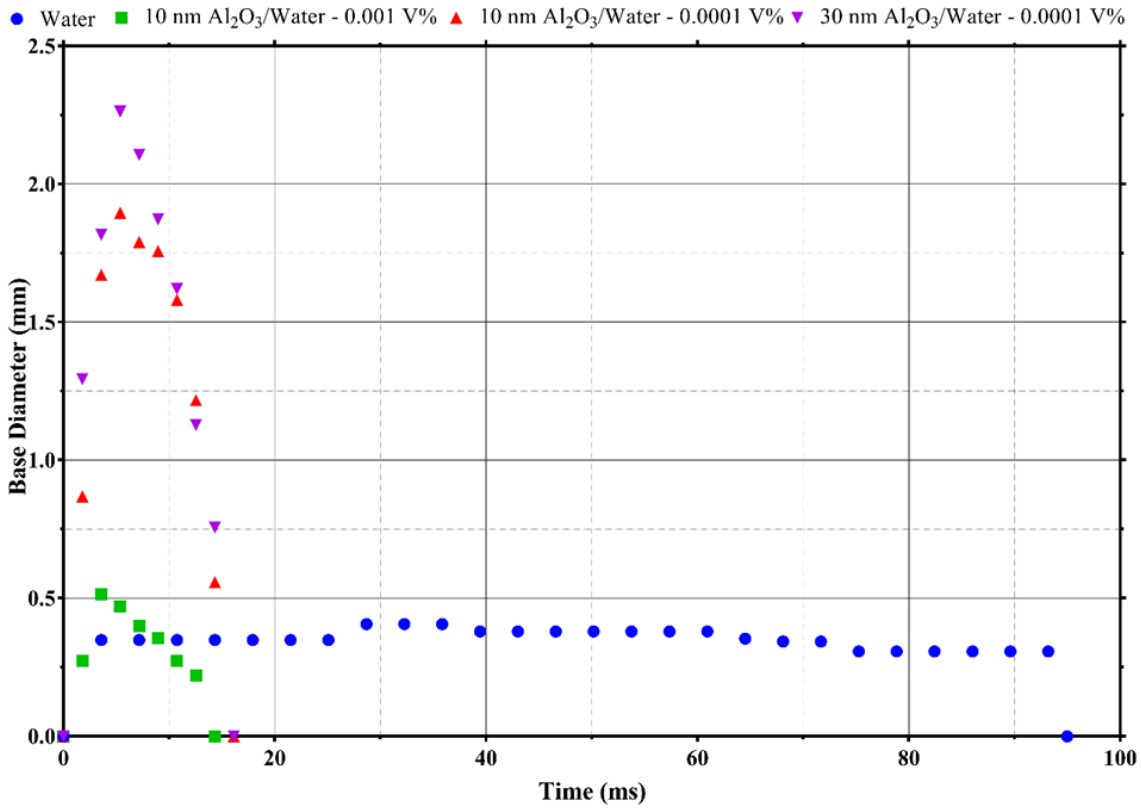

Figure 18 Comparison of bubble base diameters during boiling of nanofluids with water at 65.53 KW/m^2

During boiling of water, the base diameter of bubbles increases to a maximum of 0.40 mm. After that, the base of the bubbles remain steady for a specific time, and then they depart the surface. Compared to water, the bubbles nucleating during boiling of nanofluids have larger base dimeters. The maximum bubble base diameters for nanofluids containing 10 nm and 30 nm sized particles at the same 0.0001% concentration are 1.89 mm and 2.26 mm respectively. When the bubbles finish their growth phase, they do not hold steady at their maximum base diameter and quickly tend to departure. This behavior is observed for all the nanofluids as shown in Fig.18.

The measured average bubble equivalent diameters during boiling of water and nanofluids at 65.53 KW/m^2 are presented in Fig.19.

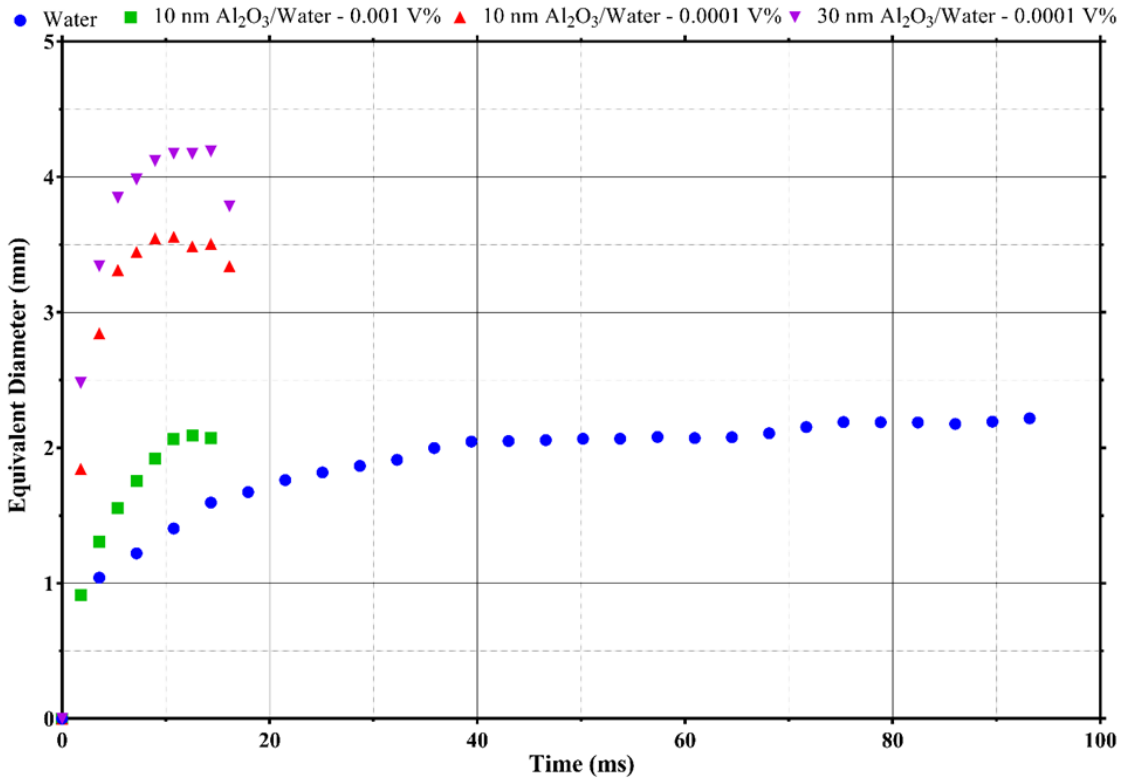

Figure 19 Comparison of bubble equivalent diameters during boiling of nanofluids with water at 65.53 KW/m^2

The bubbles formed during boiling of water steadily grow in size to a maximum equivalent diameter of 2.2 mm and depart the surface. The growth trend is similar in the nanofluid at 0.001% containing 10 nm sized particles. The maximum equivalent diameter is about 2.09 mm. For the 0.0001% concentrated nanofluids, a significant increase in the size of the bubbles is observed, irrespective of the size of nanoparticles. The bubble growth rate is high as it nucleates and the maximum equivalent diameters of bubbles formed in nanofluids containing 10 nm and 30 nm sized particles are 3.55 mm and 4.19 mm respectively. It is evident that at this higher heat flux, the effect of nanofluid particle size

on the bubble dynamics is less significant as compared to the nanofluid concentration. A higher bubble growth rate can be observed in lower concentrated nanofluids as compared to water irrespective of particle size. However in higher concentrated nanofluid, the bubble growth rate is some-what higher than that of water.

The measured contact angles during boiling of water and nanofluids at 65.53 KW/m^2 are as shown in Fig.20. During boiling of water, the bubble grows in size with an average receding contact angle of 28° and departs the surface with an average advancing contact angle of 34°. During boiling of nanofluids containing 10 nm and 30 nm sized particles, the contact angles of the bubbles are higher when compared to water. For 10 nm-0.0001 vol% nanofluid, the average receding contact angle of the bubble is 29° and the average advancing contact angle is 42°. Similarly when the nanoparticle size is increased from 10 nm to 30 nm, the average receding contact angle is 30° and the average advancing contact angle is 43°. For 10 nm-0.001 vol% nanofluid, the bubbles grow in size with an average receding contact angle of 36° and departs with an average advancing contact angle of 23°. At this heat flux, the higher concentrated nanofluid causes anomalous contact angle dynamics as the advancing contact angle is found to be lower than the receding contact angle.

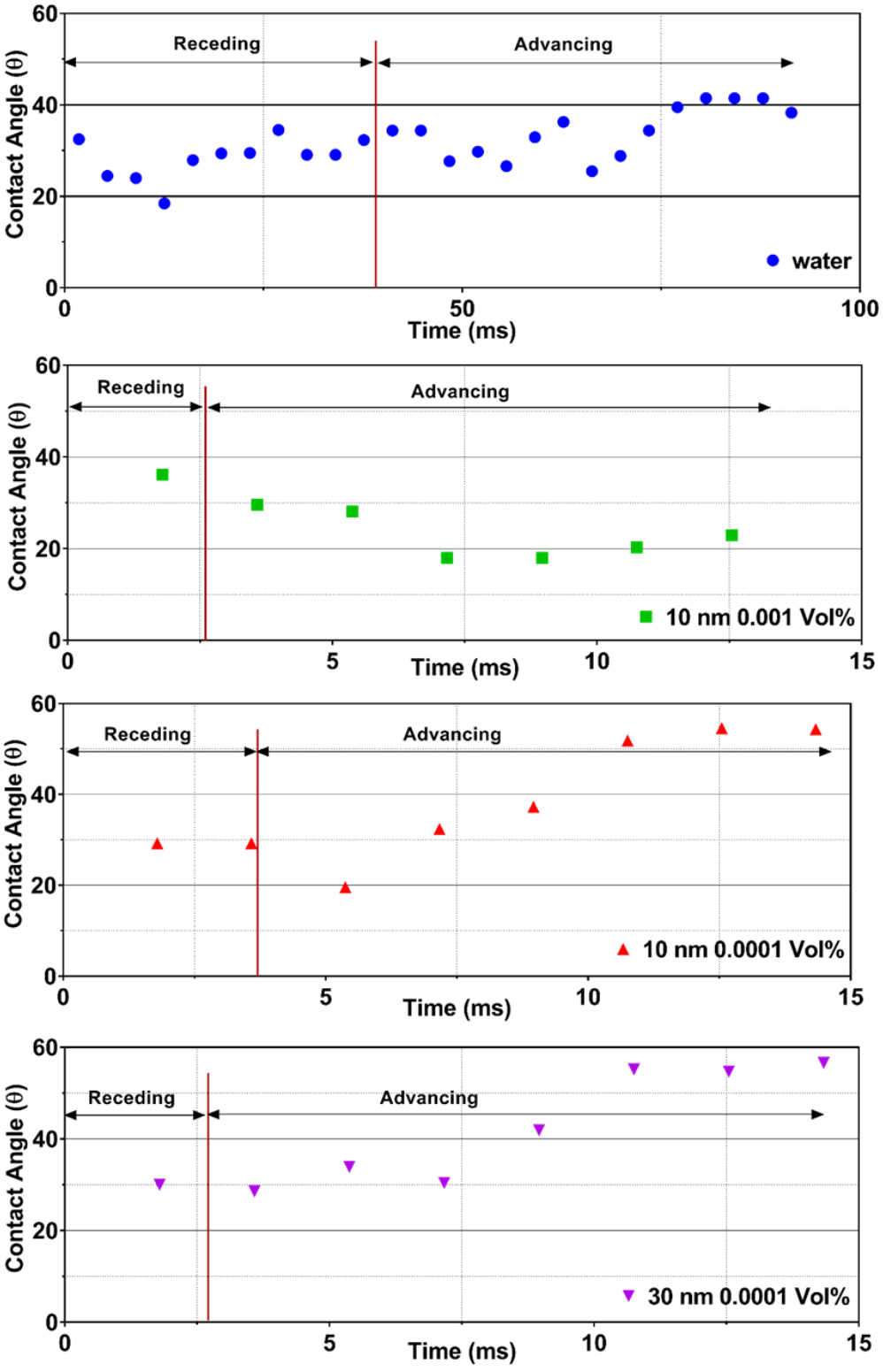

Figure 20 Comparison of bubble contact angles during boiling of nanofluids with water at 65.53 KW/m^2

Micro Layer Evaporation

During bubble growth various mechanisms transfer heat from the surface to the bubble as shown in Fig.21.

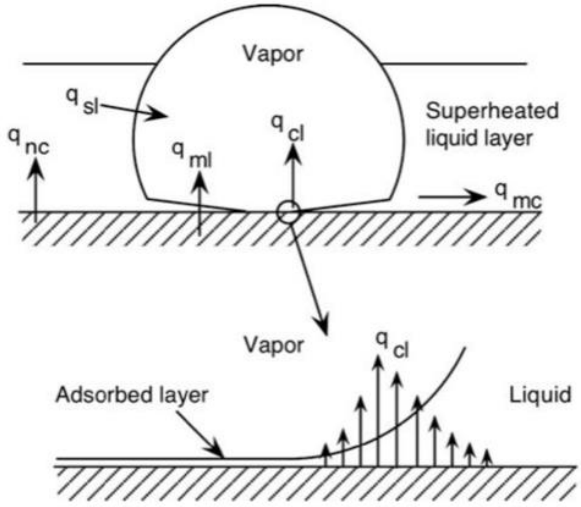

Figure 21 Heat transfer mechanisms during bubble growth [47]

A layer of liquid between the quickly growing hemispherical bubble and the wall is defined as the microlayer. Evaporation of this microlayer (q_{ml}) contributes to the bubble growth. Due to partial dry out of the microlayer, another mechanism (q_{cl}) at the three-phase contact line also contributes to the bubble growth. The thermal boundary layer at surrounding the bubble cap also evaporates (q_{sl}). In addition to these evaporation mechanisms, background natural convection (q_{nc}) and micro convection (q_{mc}) also contribute to the boiling heat transfer due to the agitation of the liquid adjacent to the bubble and disruption in the natural convection boundary layer.

In this study, the average energy transferred per bubble due to microlayer evaporation has been calculated by using the model proposed by Benjamin & Balakrishnan[48].

According to this model,

$$Q_{ME} = \rho_l h_{fg} V_{ME} \tag{14}$$

The volume of the microlayer V_{ME} :

$$V_{ME} = \sum_{t=0}^{t_g} A_{m,t}.\delta_t \tag{15}$$

Where $A_{m,t}$ and δ_t are the instantaneous area and thickness of the microlayer and t_g is the growth time of the bubbles.

The area of the microlayer can be written as:

$$A_{m,t} = \frac{\pi}{4} D_b^2 \phi \tag{16}$$

Where $\phi = 0.2$, which is the ratio of diameter of dry area under bubble to the diameter of the bubble.

The microlayer thickness is:

$$\delta_t = \frac{2\gamma}{3t}\sqrt{\frac{\alpha_l}{\pi}}\left(t_g\sqrt{t_g} - t\sqrt{t}\right) \tag{17}$$

Where $\gamma = \sqrt{\frac{k_{Cu}\rho_{Cu}C_{p.Cu}}{k_l\rho_l C_{p.l}}}$

The properties of nanofluids are similar to that of water due to their dilute concentrations. Hence for all the calculations, same fluid properties are used. Since the growth time and the bubble diameters are measured from the images obtained, no additional correlations were used. The calculated energy transferred per bubble due to microlayer evaporation during boiling of nanofluids and water are shown in Table 2.

Table 2 Energy transferred to the bubble due to microlayer evaporation

	Heat flux-45.82 KW/m^2		Heat flux-65.53 KW/m^2	
	Microlayer Volume (m^3)	Energy transferred(J)	Microlayer Volume (m^3)	Energy transferred (J)
Water	2.4E-07	522.61	5.2E-08	111.55
10 nm Al_2O_3/water at 0.0001 Vol%	4.9E-08	106.62	7.1E-09	15.30
10 nm Al_2O_3/water at 0.001 Vol%	2.8E-08	59.62	1.2E-09	2.68
30 nm Al_2O_3/water at 0.0001 Vol%	4.4E-09	9.43	1.0E-08	22.42

As seen in the table above, the energy conveyed by microlayer evaporation is higher for water when compared to nanofluids. This is due to the possible deposition of nano particles on the surface, thereby changing the surface conditions, liquid conductivity and thereby bubble growth characteristics. This could also explain the overall deterioration of the wall heat transfer in these boiling regimes.

CHAPTER VI. CONCLUSIONS

In this study, pool boiling experiments have been conducted using Al_2O_3/water nanofluids at 0.0001% and 0.001% concentrations containing 10 nm and 30 nm sized nanoparticles. During nanofluid boiling, the bubble base diameter, bubble equivalent diameter and bubble contact angles at 45.82 KW/m^2 and 65.53 KW/m^2 are measured and compared with that of water. The following conclusions can be drawn from this study:

1. At the applied heat flux range of 25-150 KW/m^2, deterioration in wall heat transfer during boiling of nanofluids was observed when compared to water.
2. During nanofluid boiling, the bubbles depart significantly faster when compared to water at 45.82 KW/m^2 and 65.53 KW/m^2.
3. At the low heat flux of 45.82 KW/m^2, the effect of nanofluid particle size on the bubble dynamics is found to be more significant as compared to the nanofluid concentration. However at heat flux of 65.53 KW/m^2, the effect of nanofluid particle size is less significant.
4. At higher nanofluid concentration of 0.001%, deposition of nanoparticles on the surface causes anomalous contact angle dynamics at both the heat fluxes.
5. The energy transferred to the bubble due to microlayer evaporation at the applied heat fluxes of 45.82 and 65.53 KW/m^2 is found to be significantly more during boiling of water as compared to nanofluids.

REFERENCES

[1] A. Faghri, Y. Zhang, and J. R. Howell, “Advanced Heat and Mass Transfer 8.2 Pool Boiling Regimes Transport Phenomena in Multiphase Systems.” [Online]. Available: http://www.thermalfluidscentral.org/e-resources/download.php?id=1.

[2] W. M. Rohsenow, “A method of correlating heat transfer data for surface boiling of liquids,” 1952.

[3] K. Stephan and M. Abdelsalam, “Heat-transfer correlations for natural convection boiling,” *Int. J. Heat Mass Transf.*, vol. 23, no. 1, pp. 73–87, Jan. 1980.

[4] M. G. Cooper, “Saturation Nucleate Pool Boiling - A Simple Correlation,” in *First U.K. National Conference on Heat Transfer*, Elsevier, 1984, pp. 785–793.

[5] S. K. Das, N. Putra, and W. Roetzel, “Pool boiling characteristics of nano-fluids,” *Int. J. Heat Mass Transf.*, vol. 46, no. 5, pp. 851–862, Feb. 2003.

[6] S. K. Das, N. Putra, and W. Roetzel, “Pool boiling of nano-fluids on horizontal narrow tubes,” *Int. J. Multiph. Flow*, vol. 29, no. 8, pp. 1237–1247, Aug. 2003.

[7] V. Trisaksri and S. Wongwises, “Nucleate pool boiling heat transfer of TiO2–R141b nanofluids,” *Int. J. Heat Mass Transf.*, vol. 52, no. 5–6, pp. 1582–1588, Feb. 2009.

[8] M. M. Sarafraz and F. Hormozi, “Nucleate pool boiling heat transfer characteristics of dilute Al2O3–ethyleneglycol nanofluids,” *Int. Commun. Heat Mass Transf.*, vol. 58, pp. 96–104, Nov. 2014.

[9] P. Naphon and C. Thongjing, “Pool boiling heat transfer characteristics of refrigerant-nanoparticle mixtures,” *Int. Commun. Heat Mass Transf.*, vol. 52, pp. 84–89, Mar. 2014.

[10] D. Wen and Y. Ding, “Experimental investigation into the pool boiling heat transfer of aqueous based γ-alumina nanofluids,” *J. Nanoparticle Res.*, vol. 7, no. 2–3, pp. 265–274, Jun. 2005.

[11] S. Soltani, S. G. Etemad, and J. Thibault, “Pool boiling heat transfer performance of Newtonian nanofluids,” *Heat Mass Transf.*, vol. 45, no. 12, pp. 1555–1560, Oct.

2009.

[12] S. Zeinali Heris, “Experimental investigation of pool boiling characteristics of low-concentrated CuO/ethylene glycol-water nanofluids,” *Int. Commun. Heat Mass Transf.*, vol. 38, no. 10, pp. 1470–1473, 2011.

[13] M. Kole and T. K. Dey, “Thermophysical and pool boiling characteristics of ZnO-ethylene glycol nanofluids,” *Int. J. Therm. Sci.*, vol. 62, pp. 61–70, Dec. 2012.

[14] M. R. Raveshi, A. Keshavarz, M. S. Mojarrad, and S. Amiri, “Experimental investigation of pool boiling heat transfer enhancement of alumina–water–ethylene glycol nanofluids,” *Exp. Therm. Fluid Sci.*, vol. 44, pp. 805–814, Jan. 2013.

[15] G. P. Narayan, K. B. Anoop, and S. K. Das, “Mechanism of enhancement/deterioration of boiling heat transfer using stable nanoparticle suspensions over vertical tubes,” *J. Appl. Phys.*, vol. 102, no. 7, 2007.

[16] M. Chopkar, A. K. Das, I. Manna, and P. K. Das, “Pool boiling heat transfer characteristics of ZrO2–water nanofluids from a flat surface in a pool,” *Heat Mass Transf.*, vol. 44, no. 8, pp. 999–1004, Jun. 2008.

[17] A. Suriyawong and S. Wongwises, “Nucleate pool boiling heat transfer characteristics of TiO2–water nanofluids at very low concentrations,” *Exp. Therm. Fluid Sci.*, vol. 34, no. 8, pp. 992–999, Nov. 2010.

[18] D. Wen, M. Corr, X. Hu, and G. Lin, “Boiling heat transfer of nanofluids: The effect of heating surface modification,” *Int. J. Therm. Sci.*, vol. 50, no. 4, pp. 480–485, Apr. 2011.

[19] D. Wen, “Influence of nanoparticles on boiling heat transfer,” *Appl. Therm. Eng.*, vol. 41, pp. 2–9, 2012.

[20] O. Ahmed and M. S. Hamed, “Experimental investigation of the effect of particle deposition on pool boiling of nanofluids,” *Int. J. Heat Mass Transf.*, vol. 55, no. 13–14, pp. 3423–3436, Jun. 2012.

[21] Z. G. Xu and C. Y. Zhao, “Influences of nanoparticles on pool boiling heat transfer in porous metals,” *Appl. Therm. Eng.*, vol. 65, no. 1–2, pp. 34–41, Apr. 2014.

[22] X. Tang, Y.-H. Zhao, and Y. Diao, “Experimental investigation of the nucleate pool boiling heat transfer characteristics of δ-Al2O3-R141b nanofluids on a horizontal plate,” *Exp. Therm. Fluid Sci.*, vol. 52, pp. 88–96, Jan. 2014.

[23] M. M. Sarafraz and F. Hormozi, “Pool boiling heat transfer to dilute copper oxide aqueous nanofluids,” *Int. J. Therm. Sci.*, vol. 90, pp. 224–237, 2015.

[24] J. T. Cieśliński and T. Z. Kaczmarczyk, “Pool Boiling of Water–Al2O3 and Water–Cu Nanofluids Outside Porous Coated Tubes,” *Heat Transf. Eng.*, vol. 36, no. 6, pp. 553–563, Apr. 2015.

[25] T. Sayahi and M. Bahrami, “Investigation on the Effect of Type and Size of Nanoparticles and Surfactant on Pool Boiling Heat Transfer of Nanofluids,” *J. Heat Transfer*, vol. 138, no. 3, p. 031502, Nov. 2015.

[26] S. M. You, J. H. Kim, and K. H. Kim, “Effect of nanoparticles on critical heat flux of water in pool boiling heat transfer,” *Appl. Phys. Lett.*, vol. 83, no. 16, pp. 3374–3376, Oct. 2003.

[27] P. Vassallo, R. Kumar, and S. D’Amico, “Pool boiling heat transfer experiments in silica–water nano-fluids,” *Int. J. Heat Mass Transf.*, vol. 47, no. 2, pp. 407–411, Jan. 2004.

[28] I. C. Bang and S. Heung Chang, “Boiling heat transfer performance and phenomena of Al2O3–water nano-fluids from a plain surface in a pool,” *Int. J. Heat Mass Transf.*, vol. 48, no. 12, pp. 2407–2419, Jun. 2005.

[29] H. Kim, J. Kim, and M. H. Kim, “Effect of nanoparticles on CHF enhancement in pool boiling of nano-fluids,” *Int. J. Heat Mass Transf.*, vol. 49, no. 25–26, pp. 5070–5074, Dec. 2006.

[30] S. J. Kim, I. C. Bang, J. Buongiorno, and L. W. Hu, “Surface wettability change during pool boiling of nanofluids and its effect on critical heat flux,” *Int. J. Heat Mass Transf.*, vol. 50, no. 19–20, pp. 4105–4116, Sep. 2007.

[31] Z.-H. Liu, J.-G. Xiong, and R. Bao, “Boiling heat transfer characteristics of nanofluids in a flat heat pipe evaporator with micro-grooved heating surface.”

[32] J. S. Coursey and J. Kim, “Nanofluid boiling: The effect of surface wettability,” *Int. J. Heat Fluid Flow*, vol. 29, no. 6, pp. 1577–1585, Dec. 2008.

[33] Z. Liu and L. Liao, “Sorption and agglutination phenomenon of nanofluids on a plain heating surface during pool boiling,” *Int. J. Heat Mass Transf.*, vol. 51, no. 9–10, pp. 2593–2602, May 2008.

[34] M. N. Golubovic, H. D. Madhawa Hettiarachchi, W. M. Worek, and W. J.

Minkowycz, “Nanofluids and critical heat flux, experimental and analytical study,” *Appl. Therm. Eng.*, vol. 29, no. 7, pp. 1281–1288, May 2009.

[35] R. Kathiravan, R. Kumar, A. Gupta, and R. Chandra, “Characterization and Pool Boiling Heat Transfer Studies of Nanofluids,” *J. Heat Transfer*, vol. 131, no. 8, p. 081902, 2009.

[36] K. J. Park, D. Jung, and S. E. Shim, “Nucleate boiling heat transfer in aqueous solutions with carbon nanotubes up to critical heat fluxes,” *Int. J. Multiph. Flow*, vol. 35, no. 6, pp. 525–532, 2009.

[37] Z.-H. Liu, X.-F. Yang, and J.-G. Xiong, “Boiling characteristics of carbon nanotube suspensions under sub-atmospheric pressures,” *Int. J. Therm. Sci.*, vol. 49, no. 7, pp. 1156–1164, Jul. 2010.

[38] S. M. Kwark, R. Kumar, G. Moreno, J. Yoo, and S. M. You, “Pool boiling characteristics of low concentration nanofluids,” *Int. J. Heat Mass Transf.*, vol. 53, no. 5–6, pp. 972–981, Feb. 2010.

[39] M. Kole and T. K. Dey, “Investigations on the pool boiling heat transfer and critical heat flux of ZnO-ethylene glycol nanofluids,” *Appl. Therm. Eng.*, vol. 37, pp. 112–119, May 2012.

[40] M. M. Sarafraz, T. Kiani, and F. Hormozi, “Critical heat flux and pool boiling heat transfer analysis of synthesized zirconia aqueous nano-fluids,” *Int. Commun. Heat Mass Transf.*, vol. 70, pp. 75–83, Jan. 2016.

[41] C.-K. Huang, C.-W. Lee, and C.-K. Wang, “Boiling enhancement by TiO2 nanoparticle deposition,” *Int. J. Heat Mass Transf.*, vol. 54, no. 23–24, pp. 4895–4903, Nov. 2011.

[42] S. Lee Song, J. Hyung Lee, and S. Heung Chang, “CHF enhancement of SiC nanofluid in pool boiling experiment,” *Exp. Therm. Fluid Sci.*, vol. 52, pp. 12–18, 2014.

[43] R. Kamatchi, S. Venkatachalapathy, and C. Nithya, “Experimental investigation and mechanism of critical heat flux enhancement in pool boiling heat transfer with nanofluids,” *Heat Mass Transf.*, vol. 52, no. 11, pp. 2357–2366, Nov. 2016.

[44] R. Kathiravan, R. Kumar, A. Gupta, R. Chandra, and P. K. Jain, “Pool boiling characteristics of multiwalled carbon nanotube (CNT) based nanofluids over a flat

plate heater," *Int. J. Heat Mass Transf.*, vol. 54, no. 5–6, pp. 1289–1296, Feb. 2011.

[45] Y. H. Diao, C. Z. Li, Y. H. Zhao, Y. Liu, and S. Wang, "Experimental investigation on the pool boiling characteristics and critical heat flux of Cu-R141b nanorefrigerant under atmospheric pressure," *Int. J. Heat Mass Transf.*, vol. 89, pp. 110–115, Oct. 2015.

[46] S. Vafaei, "Nanofluid pool boiling heat transfer phenomenon," *Powder Technol.*, vol. 277, pp. 181–192, Jun. 2015.

[47] J. Kim, "Review of nucleate pool boiling bubble heat transfer mechanisms," *International Journal of Multiphase Flow*. 2009.

[48] R. J. Benjamin and A. R. Balakrishnan, "Nucleate pool boiling heat transfer of pure liquids at low to moderate heat fluxes," *Int. J. Heat Mass Transf.*, vol. 39, no. 12, pp. 2495–2504, 1996.